Study of the encapsulation of healing agents for autonomous self-healing coatings.

Sven Pletincx

Master thesis submitted under the supervision of
Prof. dr. ir. Iris De Graeve

The co-supervision of
Prof. dr. ir. Herman Terryn

Academic year
2013-2014

In order to be awarded the Master's Degree in
Applied Sciences and Engineering: Materials and Chemistry

Preface

This master thesis allowed me to further investigate the topic of self-healing materials that fascinates me very much. The idea of materials that have undergone damage have a build-in capability to repair the damage and to restore the functionality of the coating intrigues me. Given the attention this hot-topic gets from industry and the high relevance for sustainable material development, made me enjoy working on this topic. Therefore I would like to thank Professor Iris De Graeve and Professor Herman Terryn for the opportunity to work on this topic and providing me with their help and guidance throughout this project. Further I would like to thank others who were part of the accomplishment of this thesis.

Hilke Verbruggen who supported and helped me a lot this year in finding solutions to all the different problems that had to be tackled. And who made the trip to the company Toseda in the Czech Republic an unforgettable event in my academic career.

Dr. Makoto Chiba who also made the trip to Toseda an unforgettable stay and who learned me a lot about the Japanese culture.

Tomas Vlcek, who taught me how to make microcapsules and provided me with a lot of ideas and support. I also want to thank him for being such a great host while we were at the Czech Republic and for showing us all the nice places in Pardubice.

Dr. Alexandros Kakaroglou who supported me and provided me a lot of help in performing EIS measurements.

Dr. Tom Hauffman who gave me a lot of advice and who provided me a lot of help in performing AFM measurements.

Alexander Lutz who gave me a lot of advice during the progress of this thesis.

Professor Guy Van Assche, for his patience, advice and for teaching me how to use a TGA and especially how to fix one.

I want to thank everybody at the SURF and FYSC department who have lent me a helping hand.

A special thanks goes to my classmates; Mats, Robrecht, Alicia and Avdyl who made my education period at VUB an unforgettable life experience. My deepest gratitude goes to Evelyne Demol, who was always there to help me finish a paper or to explain me things I didn't understand.

A last big thanks goes to my parents, my two sisters and my girlfriend who supported me all the time and who made it possible for me to study. Without them, all this wouldn't be possible.

Abstract

English

Metals are widely used in building and construction because of their good properties. However, their main drawback is their susceptibility to corrosion. Various methods to protect the metal substrate exist but one of the most common methods is the application of an organic coating. These organic coatings extend the lifetime of the metal substrate by forming a barrier against the aggressive environment, but whenever a coating is damaged it loses this protective barrier property and the substrate can corrode. In order to further increase the lifetime of the underlying metallic substrate, a new approach is being developed, i.e. self-healing polymeric coatings, which can heal sustained damages. In this work, the concept of autonomous self-healing polyurethane coatings is considered. These coatings make use of microcapsules that contain a liquid healing agent that can react with water from the atmosphere. These microcapsules dispersed in a polyurethane coating will crack open when damage occurs and the liquid healing agent flows into the defect. The coatings are called autonomous because no external trigger or any kind of human intervention is needed for healing to occur.

In the first part of the present work, different types of microcapsules are synthesized and analysed. The first step in the production of microcapsules is the synthesis of prepolymers, which are based on toluene diisocyanate (TDI). By using three different types of polyol, three different types of prepolymer are synthesized. These polyols are the triol glycerol, the diol 1,4-butanediol and the triol castor oil. The second step is to use the synthesized prepolymer mixtures to perform an interfacial polymerization reaction in an oil-in-water emulsion in order to create microcapsules. As the healing agent isophorone diisocyanate (IPDI) is encapsulated, which is an aliphatic diisocyanate that can react with water to form eventually polyurea. These capsules are studied by means of electron microscopy, Fourier Transform Infrared Spectroscopy (FTIR) and thermal analysis. The relative reactivity with water from the environment with two aliphatic diisocyanates is investigated. It is also attempted to encapsulate a second aliphatic diisocyanate, hexamethylene diisocyanate (HDI) in a polyurethane shell.

In the second part of the present work, the microcapsules produced with the glycerol TDI based prepolymer and glycerol as polyol chain extender are dispersed in polyurethane coatings. Several polyurethane coatings are synthesized containing different concentrations of these IPDI containing microcapsules. After the synthesis of the coatings, their quality and ability to self-heal are evaluated by different techniques such as Field Emission Scanning Electron Microscopy (FE SEM), Electrochemical Impedance Spectroscopy (EIS) and Atomic Force Microscopy (AFM).

This study shows the formation of different types of spherical microcapsules and that the healing agent IPDI can be successfully encapsulated. Unfortunately the used coating formulation results in relatively poor quality coatings; hence, further optimization is required. Despite this fact, there are however indications of healing of an applied defect observed by means of EIS.

Nederlands
Metalen worden wereldwijd gebruikt in de constructie van gebouwen omwille van hun goede eigenschappen. Hun voornaamste nadeel is echter hun gevoeligheid voor corrosie. Er bestaan verscheidene methodes om de metalen substraten te beschermen maar één van de meest gebruikte methodes is het aanbrengen van een organische coating. Deze organische coatings verlengen de levensduur van het metalen substraat door een barrière te vormen tegen de agressieve omgeving, maar wanneer de coatings beschadigd zijn, verliezen ze deze beschermende barrière-eigenschap en kan het substraat corroderen. Om de levensduur van het onderliggende substraat verder te verlengen, werd er een nieuwe aanpak ontwikkeld, namelijk de zelfhelende polymeer coatings. Deze kunnen opgelopen schade helen. In dit werk wordt het concept van autonome zelfhelende polyurethaan coatings bekeken. Deze coatings maken gebruik van microcapsules, die een vloeibaar helend middel bevatten dat kan reageren met water uit de lucht. Deze microcapsules zijn gedispergeerd in een polyurethaan coating en zullen open breken wanneer er een beschadiging in de coating optreedt. Het vloeibaar helend middel zal dan in de beschadiging vloeien en reageren. Deze coatings worden autonoom genoemd omdat ze geen externe trigger of enige andere vorm van menselijke interventie nodig hebben voor herstel.

In het eerste deel van dit werk worden verschillende soorten microcapsules gesynthetiseerd en geanalyseerd. De eerste stap in de productie van microcapsules is de synthese van de prepolymeren, gebaseerd op tolueen diisocyanaat (TDI). Door drie verschillende soorten polyol te gebruiken worden drie verschillende typen prepolymeer gesynthetiseerd. Deze polyolen zijn het triol glycerol, het diol 1,4-butaandiol en het triol castorolie. De tweede stap is het gesynthetiseerde prepolymeermengsel te gebruiken om een grensvlak polymerisatie reactie in een olie-in-water emulsie uit te voeren om microcapsules te maken terwijl het helend middel isophorone diisocyanaat (IPDI) wordt ingekapseld. IPDI is een alifatisch diisocyanaat dat kan reageren met water om uiteindelijk polyurea te vormen. Deze capsules worden geanalyseerd met elektron microscopie, Fourier Transform Infrarood Spectroscopie (FTIR) en via thermische analyse. De relatieve reactiviteit met water vanuit de atmosfeer met twee alifatische diisocyanaten is onderzocht. Het is ook geprobeerd om dit tweede alifatisch diisocyanaat in te kapselen in een polyurethaan capsule.

In het tweede deel van dit werk worden de microcapsules, die geproduceerd zijn met het glycerol TDI prepolymeer en met glycerol als polyol keten-verlenger, gedispergeerd in een polyurethaan coating. Verscheidene polyurethaan coatings met verschillende concentraties van deze IPDI bevattende microcapsules zijn gesynthetiseerd. Na de synthese van deze coatings zijn hun kwaliteit en hun zelfhelend vermogen geëvalueerd door verscheidene technieken zoals Field Emission Scanning Electron Microscopy (FE SEM), Electrochemische Impedantie Spectroscopie (EIS) en Atoomkrachtmicroscopie (AFM).

Deze studie toont de vorming van verschillende soorten sferische capsules aan en toont ook aan dat het helend middel IPDI met succes werd ingekapseld. Helaas resulteert de gebruikte coatingformulering in coatings van een relatief lage kwaliteit, vandaar dat verdere optimalisatie nodig is. Ondanks dit feit zijn er echter aanwijzingen van herstel van een toegepast defect waargenomen door middel van EIS.

Français
Les métaux sont utilisés partout dans la construction et les bâtiments en raison de leurs bonnes qualités. Cependant, leur principal inconvénient est leur sensibilité à la corrosion. Divers méthodes pour protéger le substrat métallique existent, mais l'une des méthodes les plus courantes est l'application d'un revêtement organique. Ces revêtements organiques étendent la durée de vie d'un substrat métallique en formant une barrière contre l'environnement agressif, mais à chaque fois qu'un revêtement est endommagé, il perd cette propriété de barrière protectrice et le substrat peut se corroder. Afin d'augmenter encore la durée de vie du substrat métallique sous-jacent, une nouvelle approche est en cours d'élaboration, à savoir des revêtements polymères auto-guérison, qui sont à mêmes de guérir les dommages subis. Dans ce travail, la notion de revêtements de polyuréthane auto-cicatrisants autonomes est considérée. Ces revêtements utilisent des micro-capsules contenant un agent de guérison liquide qui peut réagir à l'eau de l'atmosphère. Ces micro-capsules dispersées dans un revêtement de polyuréthane se fissurent en cas de dommage et leur continu coule dans la partie dédommagée pour y réagir. Les revêtements sont appelés autonome car ils ne nécessitent pas de déclenchement externe ou d'intervention humaine pour entamer leur tâche de guérison.

Dans la première partie du présent travail, les différents types de micro-capsules sont synthétisés et analysés. La première étape dans la production de micro-capsules est la synthèse de prépolymères qui sont basés sur la toluène diisocyanate (TDI). En utilisant trois types différents de polyol, trois types de prépolymère différents sont synthétisés. Ces polyols sont : le triol glycerol, le diol 1,4-butanediol et le triol l'huile de ricin. La deuxième étape consiste à utiliser les mélanges prépolymères synthétisés pour effectuer une réaction de polymérisation interfaciale dans une émulsion « huile-dans-eau » dans le but de créer des micro-capsules. En même temps l'agent de guérison isophorone diisocyanate (IPDI) est encapsulé. Il s'agit d'un diisocyanate aliphatique qui peut réagir avec l'eau pour former éventuellement polyurea. Ces capsules sont étudiées au moyen de la microscopie électronique, Fourier Tansform Infrared Spectroscopy (FTIR) et de l'analyse thermique. La réactivité relative à l'eau de l'environnement avec deux diisocyanates aliphatiques est étudiée. On a également tenté d'encapsuler un second diisocyanate aliphatique, hexaméthylène diisocyanate (HDI) dans une coque en polyuréthane.

Dans la deuxième partie de ce travail, les micro-capsules produites par le glycerol TDI prépolymère et par le glycerol comme agent d'allongement de le chaine polyol, sont dispersées dans des revêtements de polyuréthane. Plusieurs revêtements de polyuréthane, avec des concentrations différents de ces micro-capsules contenant IPDI, sont synthétisés. Après la synthèse des revêtements, leur qualité et leur capacité d'auto-guérison sont évaluées par différentes techniques telles que Field Emission Scanning Electron Microscopy (FE SEM), Elechtrochemical Impedance Spectroscopy (EIS) et Atomic Force Microscopy (AFM).

Cette étude démontre la formation de différents types de micro-capsules sphériques et que l'agent de cicatrisation IPDI peut être encapsulé avec succès. Malheureusement la formation du revêtement utilisé n'aboutit pas toujours au résultat envisagé : par conséquent une élaboration supplémentaire est nécessaire. Malgré ce fait, il existe cependant des indications de guérison d'un défaut appliqué, ce qui a été observé par EIS.

Table of Contents

I. Introduction

Nowadays metals and metal alloys are widely used in building and construction throughout the world because of their high strength and good functional properties. However, a major drawback of these materials is their susceptibility to corrosion. This phenomenon can be defined as a destructive attack of a material by a chemical or electrochemical reaction with its environment. Material losses and degradation of the properties of the materials are a direct result of corrosion and can even lead to dangerous situations. [1] Therefore the three main reasons to manage corrosion are safety, conservation of the materials and the economic impact. Repair and replacement costs due to corrosion related damages of structures can be 3 – 4 % of the Gross Domestic Product of an industrialized nation. It was estimated that 25 – 30% of this cost could be reduced if current technology was used efficiently. [2]

Various methods to protect materials against corrosion exist, but one of the most common and cheapest methods is the application of an organic coating. This coating is a solid phase that is mechanically or chemically attached to a much thicker structure that will also add certain functionalities. Examples of these functionalities are colour, wear resistance, thermal protection, light reflection, hydrophobicity or hydrophilicity, electrical and thermal conductivity or insulation and other functionalities that are not inherent to the substrate material along with corrosion protection. [3] Coatings extend the lifetime of a structure in corrosive environments by creating a barrier between the metal and its environment. Therefore, no electrochemical reaction that would oxidize the metal can take place. Often the applied coatings were relatively thick to have a high initial performance but when the coatings are damaged, this protection is lost. Additionally, an effective combination with corrosion inhibitors was used on metals structures from the 20th century. Cr-VI based corrosion inhibitors, chromate conversion layers and lead oxide based paints are excellent inhibitors but are also highly toxic and chromates have a carcinogenic effect. By changing the regulations the European Union banned the use of these inhibitors in many applications. Consequently, these corrosion inhibitors need to be replaced by eco-friendly inhibitors. However, up till now the provided green inhibitors have not the same efficiency as their toxic predecessors. [4]

When a conventional coating is damaged due to wear, a sudden impact or other external effects, the barrier corrosion protection can be lost. However, new approaches are being developed to increase the lifetime of metallic structures. The goal is to develop a coating without toxic inhibitors that can heal damages in order to recover the initial functionalities. This self-healing approach tries to simulate a known mechanism from nature that ensures living organism to survive in time by an active repair system. [3]

Over the past few years, different self-healing strategies have been developed. In this thesis, the focus will be on systems that can heal “autonomously” by the use of an encapsulated single healing agent (HA) that can react with the environment (e.g. humidity or oxygen) to heal the coating. It is expected that when damage

occurs in these coatings with embedded and encapsulated HA, the capsules break and the healing agent is released. HA flows in the created voids, where it reacts with the external environment. This initiates the reaction that reconstructs the coating, the damage should disappear and the coating should have healed itself autonomously.

Because coatings have a thin thickness (between 1 – 100 μm), the capsules should preferably be of submicron size. Especially when the coatings have to be transparent, the capsules may not diffract the light. However, the smaller the volume of the capsules, the smaller the amount of HA that can be encapsulated. Therefore, the risk that the void cannot be completely filled with HA exists. A proper balance should be found. Another important remark is that the capsules need to be dispersed homogeneously in the polymer matrix to get uniform properties, which is not an easy task.

Objectives of the research

In the SURF research group, up till now research on self-healing coatings was focussed on thermally triggered healing coatings [5-7] containing corrosion inhibitors.

In the present work, research is focussed for the first time on autonomous self-healing coatings that require no external stimulus for healing to occur.

In the first part of this work the aim is to synthesize capsules by interfacial polymerization of polyurethane (PU). The characterisation of the capsules and the encapsulated HA will be done by optical and electron microscopy techniques together with several thermal analysis techniques and Fourier-Transform Infrared Spectroscopy (FTIR).

In the second part of this work, the aim is to disperse the capsules in polyurethane coatings. These coatings are then evaluated on their ability to self-heal and their ability to protect the substrate against corrosion. Optical techniques to visualize the damages in the coating will be used, as well as Electrochemical Impedance Spectroscopy (EIS) and Atomic Force Microscopy (AFM) to investigate the healing.

II. Background

1. Corrosion

Corrosion is the spontaneous attack of a material by an electrochemical reaction with its environment that results in the gradual destruction of the material and possibly the creation of an unwanted substance. [1] The physical properties of a material, the mechanical properties or other properties will change due to corrosion, most of the time in a negative way. [8] For metals, corrosion is a result of material loss, which happens by dissolution due to the oxidation of a metallic element in order to render it soluble in a liquid phase. [9] Rusting is the most-known example of electrochemical corrosion. It is the corrosion of iron or iron-based alloys with the formation of iron oxide/hydroxide that has a typical brown colour. [2] It is of great importance to understand the cause and the process of corrosion to be able to prevent or reduce the negative impacts, both economical and material-related. [10] Corrosion protection can be done by several ways as will be discussed later on.

1.1. Electrochemistry

The corrosion process is an electrochemical process for metals. The phenomenon can be described by a galvanic cell. When two electrical conductors or electrodes are immersed in an electrolyte a galvanic cell is formed. This cell converts chemical energy into electrical energy by reduction-oxidation reactions (redox). The electrode can only act as a source for electrons (reduction) or a sink for electrons (oxidation) that are transferred to or from the species in the electrolyte solution.

$$O + ne^- \rightarrow R$$

Where O and R are the oxidized and reduced species, respectively. Electrons are set free from the metal by an oxidation reaction. Typically the following half-reaction takes place at the metal:

$$M \rightarrow M^{n+} + ne^-$$

This is the anodic reaction, which takes place at the anode. At the cathodic side, an oxidizing agent takes up electrons. This is called the reduction reaction or cathodic reaction. Depending on the environment of the metal, different reactions can take place. In an acidic environment, H^+-ions are reduced.

$$2H^+ + 2e^- \rightarrow H_2$$

Or, in the presence of oxygen:

$$O_2 + 4H^+ + 4e^- \rightarrow 2H_2O$$

For neutral and basic solutions that contain oxygen the following half-reaction occurs:

$$O_2 + 2H_2O + 4e^- \rightarrow 4(OH^-)$$

Because metal ions can exist in more than one valence state, the reduction half-reaction can also be represented as follows:

$$M^{n+} + e^- \rightarrow M^{(n-1)+}$$

Or when the metal ions are reduced totally to a neutral metallic state:

$$M^{n+} + ne^- \rightarrow M$$

An overall electrochemical reaction consists of at least one reduction and one oxidation reaction and will be the sum of them. [8] [10]

1.2. Thermodynamics

All reactions that happen spontaneously have a Gibbs free energy change (ΔG) that is negative. An important tool in corrosion science is the Pourbaix diagram, which was created by Marcel Pourbaix in 1945. The Pourbaix diagram or E-pH diagram identifies the (equilibrium) phases of the studied aqueous electrochemical system that have the lowest Gibbs free energy for various potential and pH variables. In this way it can be seen whether a metal is susceptible to corrosion or not. The diagram is constructed from the potential of the metal in respect to the standard hydrogen potential and from equilibrium constants. The potential is calculated via the Nernst equation. Each line of the diagram corresponds to a thermodynamic equilibrium for some reaction with equal activities. The positions of these lines are determined by the ionic activity of the solution. [1] [10]

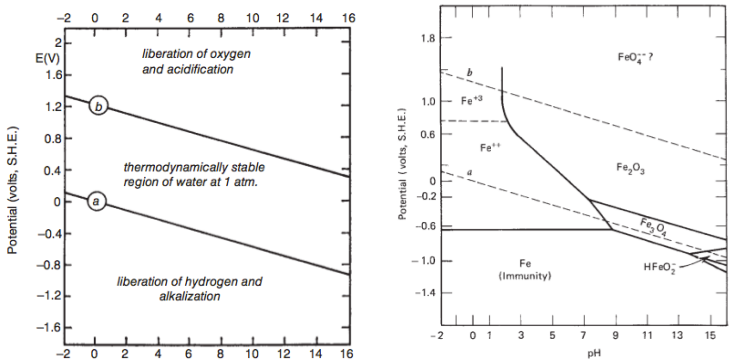

Figure 1: Pourbaix diagram of water (left) and iron (right). [9]

In the diagram of water (Figure 1) it can be seen that above line b oxygen is liberated (oxidation reaction). Below line a, hydrogen is liberated, which is the reduction reaction. In between the lines water is stable. The possibility of corrosion occurs when line a or b lies above the boundary line for oxidation of the metal. However, it is also possible that passivation occurs. If the metal ions react with oxygen, a stable oxide layer may be formed on the metal surface, which will prevent the corrosion process to continue. It is very important to remark that Pourbaix diagrams are based on thermodynamic data and that they provide no information on the kinetics and thus the rates of the reactions. The diagrams are only valid for aqueous systems, so no information on the influence of other ions (like Cl^-) is provided. [9]

1.3. Kinetics

The Pourbaix diagram plots information of systems that are at equilibrium. However, corrosion is a non-equilibrium process because there is a net current through the surface of the anode and the cathode. Therefore, the Pourbaix diagram of a metal does not provide any information on the rates of corrosion. It only gives us under which conditions the metal has a tendency to react. [1]

A simple way to express the rate of corrosion (R) involves the exposing of a clean weighed piece of metal to a corrosive environment for a specific time. After this time, the specimen is cleaned to remove the formed corrosion products and is then weighed. This allows determining the loss of mass per unit time. [8]

$$R = \frac{KW}{(\rho A t)} \left(\frac{mm}{year}\right) \quad (1)$$

With a constant K, which has a value of 87.6 if the used unit of R is millimetres per year (mm/yr), W (mg) the weight loss after exposure time t (h), ρ (g/cm^2) and A (cm^2) the density and the exposed area respectively. The rate of corrosion or corrosion penetration rate (CPR) is acceptable for most applications when it has a value smaller than 0.5 mm/year. [8]

The corrosion rate can also be expressed in terms of the current density. The current density (i) is the current per unit surface area of a material. Corrosion rate (r) can be expressed by following formula:

$$r = \frac{i}{nF} \left(\frac{mol}{m^2 * s}\right) \quad (2)$$

Where n is the number of electrons transferred and F the Faraday constant. The rates at which the metal corrodes can thus be predicted by measuring electrochemical parameters. [8]

2. Corrosion prevention

One of the easiest ways of corrosion prevention is the correct material selection once the corrosive environment is known. But due to economic reasons, it is not always possible to choose the best corrosion resistant material. Therefore, other corrosion prevention methods are designed. For example cathodic protection like sacrificial anodes or impressed current systems, the application of a metallic, inorganic or organic coating or the addition of an inhibitor to the system. [1] [10] This work will focus on organic coatings with a very particular property. This property is the ability of the coating to self-heal damages and as such increase the lifetime of the substrate.

2.1. Organic coatings

An organic coating is a thin solid layer that is attached to a thicker substrate and which adds certain properties to it. The major components of the coating are the binder and the fillers. The binder consists of resin and plasticizer and the fillers are colour or protective pigments. [11] These two major components of a coating can be combined with small amounts of other substances such as surface-active agents, driers, biocides or thickeners. The binder is the continuous phase that gives the coating its main mechanical and chemical characteristics whereas the filler is the discontinuous phase of the coating and gives additional or improved properties to the coating. [12] There are three important interactions that need to be considered:

- Coating-Substrate
- Coating-Environment
- Binder-Filler

The interaction between the coating and the substrate has an impact on the adhesion properties and therefore on the long-term (corrosion) protection of the underlying substrate. The compatibility between the binder and the filler is a key factor to improve the mechanical properties of the coating and to decrease the tendency of degradation due to external factors. And finally, the binder-filler interaction is important for film formation and densification of the coating. Also the degradation resistance to external agents such as water and oxygen is altered. [3] [11]

The binder is either a three-dimensional network of covalently bonded polymer segments (thermoset [13] e.g. polyurethane, epoxy, etc.) or a system of entangled chains (thermoplastic e.g. acrylic resin, polyester, etc.). Because of their good properties before, during and after use, thermosets are the most common applied binders and their network architecture offers a high resistance to chemicals, solvents and mechanical stresses in comparison with thermoplastics. [3] [11]

2.2. Multilayer coatings

The application of a coating can be done as a single layer, but in general they are applied as layered systems. Each layer of the coating is optimized to have certain functionalities. The multilayer coating that we want to achieve consists of three layers. (I) A conversion coating (e.g. Ti conversion) above the substrate to assure a good adhesion of the polymer layer and to provide active corrosion protection, (II) a primer layer and (III) a topcoat. [11] [14]

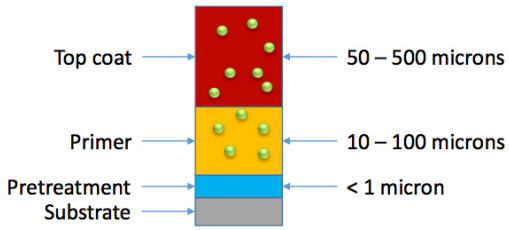

Figure 2: Schematic representation of an ideally coated substrate with microcapsules. [14]

2.3. Damages in coatings

Ideally, coatings retain their original properties (like colour, corrosion protection, etc.) during the whole lifetime of the application. Unfortunately, this is not the case. Due to mechanical causes such as impacts, scratches, thermal cycles and fatigue as well as chemical reasons such as UV radiation, acid and alkali aggressions, moisture and oxygen influences and thermo-oxidation, the coating will undergo weathering and ageing. The result of these degradation processes is the loss of one or several functionalities of the coating and this is mainly defined as "damage". [3]

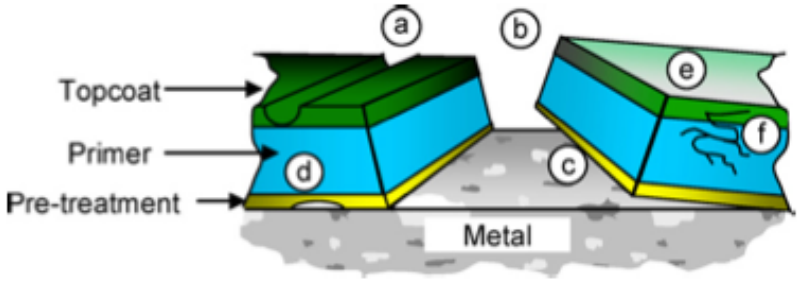

Figure 3: Common damages in an organic coating. [3]

The most common types of damage that can affect a coating are represented in Figure 3. These types of damages are superficial mechanical or chemical damage (a), a mechanical damage that reaches completely to the substrate (b), delamination of the coating next to the damaged area (c), local delamination (d), degradation of an aesthetic property like colour (e) and crazing micro-cracks (f). [3]

When a superficial scratch is disrupting the surface of the material, the visual appearance of the coating is changing and when a crack penetrates through the coating, the protective function of the coating is lost. These are two examples of an immediate damage on the scale of the coating itself and are described as macroscopic damages. However, it is important to understand that there is microscopic damage associated to the macroscopic damage. When looking at the example of the crack in the coating, it is obvious that the crack could not arise if not the coating constituents on the microscopic scale (like the molecular network segments or even the filler) have been broken. In between the two scales a third scale can be defined. In the crack formation process, the mesoscopic scale is defined as the yielding and crazing that leads to the initiation and propagation of a crack. [11]

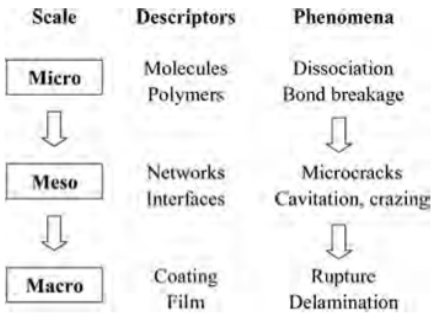

Figure 4: Damage scales. [15]

It is also important to define an imminent loss of a function as damage. When looking again at the example of the crack, the rupture can be due to the build-up of internal stresses besides the obvious stresses, which are directly related to an immediate damage. Firstly, there can be internal stresses due to shrinking as a result of diminished reaction volume and the loss of hydrodynamic volume. Secondly, there can be internal stresses in the polymer coating and interfacial stresses between the coating and the substrate due to the difference in thermal expansion coefficient and in combination with the thermal history of the coating. And finally, previous external stresses may have left traces on the microscopic and mesoscopic level, which have not been revealed on the macroscopic level. [15]

Currently, a damage prevention method is used in the design of structures. Although this is a very useful concept, damage during use can never be excluded. This means that currently made structures need periodic inspections to monitor damage development. Any damage that is observed requires an action and this costs money. An alternative to this concept is damage recovery. [11]

2.4. Damage recovery

When looking at the damage recovery of self-healing coatings, the same micro-meso-macro hierarchy has to be kept in mind. The recovery of damage always involves material transport in the coating. This can be due to the individual motion of small molecules or the collective motion due to viscous or viscoelastic flow of the polymer binder. The self-healing can take place within the bulk of the polymer binder or between the bulk of the coating and the three interfaces mentioned above. [11] [15]

However, the limiting factor of self-healing is the material transport and it is therefore important to limit the need for this factor in the self-healing process. An appropriate timing is of great importance because if enough time is given to the damage to propagate, it will reach the macroscopic scale (e.g. a crack). Obviously, it will then take more material transport to heal this defect and this can be too demanding for the self-healing polymer coating. [11] [15]

The defect should be prevented from growing by stopping crazing on the mesoscopic scale or even the initiation of the crack on the microscopic scale and therefore much less material transport is needed to keep the coating in an unspoiled state on the macroscopic level. This is the principle of pre-emptive healing. The damage process can be considered as a process that starts on the microscopic scale and propagates to the mesoscopic scale. Finally, this will lead to the loss of a function on the macroscopic scale. Therefore, preventing damage from escalating to the next level is an obvious strategy for self-healing coatings. Pre-emptive can be interpreted such that the healing action starts before there is any damage, however this is not the way this should be interpreted. The correct interpretation is that healing starts before the damage has reached the macroscopic level, when a property of the coating is affected. At the level of the macroscopic viewer, the imminent damage in the coating is prevented by an invisible healing action. [11] [15]

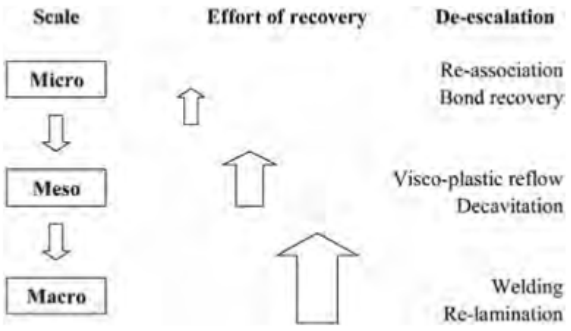

Figure 5: recovery effort and recovery method on different scales. [15]

3. Self-healing coatings

The self-healing approach depends on a number of factors. The most obvious ones are the initial requirements of the coating and the description of the functionalities that are to be restored. Also the components of the coating such as the binder and the filler are important. A third factor that has to be considered is the size scale and the type of damage. The optimal self-healing strategy depends also on the application of the coatings and their wide range of thicknesses that go from 50 nm -5 µm (pretreatment - conversion) to 50-300 µm (primer or finishing coatings in architecture, infrastructure, aerospace) to more than 500 µm (topcoat for maritime uses). [4] The last important element is the effect of the healing mechanism on the general performance of the coating. Ideally, the healing mechanism should not affect other properties to a level that is unacceptable. [3]

These factors suggest that self-healing materials require some specific properties [3]:

- A mobile phase that is stored in a container or that is intrinsically incorporated in the binder that can act as a healing agent. Only when the damage has occurred this healing agent should be active on the place of the damage.
- Externally supplied healing agents (e.g. moisture or oxygen) may be required if the healing of the damage requires new material to fill the damage volume.
- A period of reduced loading on the material may be required to allow the healing process to take place. This is the so-called recovery process.
- Externally supplied energy (like an elevated temperature, UV, kinetic energy due to high speed impacts, …) may be required to initiate the healing process by increasing the local mobility. Also the recovery period is then minimized to suitable time scales.
- Self-healing materials may also require a detection mechanism to determine the presence of damage and an activation mechanism to initiate healing.

A self-healing coating is called autonomous if damage heals automatically and no human interaction takes place and no external energy is supplied. [16]

Currently, the research on self-healing of coating functionalities is mainly focused on the partial or total recovery of the aesthetics and barrier protection, leading to an extension of the corrosion protection. But also other functionalities such as the recovery of hydrophobicity have been investigated. [17] The healing of damages like delamination at the scratched area, local delamination and colour degradation receive much less attention due to the high complexity. [3]
In this work, the focus of the self-healing is also on the aesthetic functionality and the barrier recovery to extend the lifetime of the underlying substrate and healing mechanism consist of the "gap-filling" concept. When damage occurs, an "empty" volume is created. In order to heal this defect, the created gap has to be filled. This can be done by several additive or intrinsic concepts including the release of reactive liquids that are encapsulated in containers, which is called "flow". A second concept to heal the aesthetics and barrier protection is called "re-flow" and makes use of intrinsic properties such as local network mobility, reversible covalent bonds or reversible physical networks. The last concept is "expansion", which uses external sources to supply an essential component for healing to occur. [3] The system under investigation in this work consists of encapsulated healing agents that will "flow" when damage has occurred. This concept is further elaborated below.

3.1. Self-healing by encapsulated and embedded healing agents

Various approaches by using the reflow concept for achieving self-healing have been proven over the past decade. For example reversible chemistry approaches such as Diels-Alder [18-20], reversible covalent bonds [21], sulfur based chemistry [22] and reversible non-covalent bonds like ionomers [23-25], hydrogen-bonds [26][27], donor-acceptor stacking interactions [28] and retarded elasticity [29][30] have been proven. However, the most of these systems have chemical and mechanical limitations, which may limit or prevent their use as a self-healing coating. [16]

Therefore, an alternative way to implement a self-healing system in a coating is to use the flow concept. The most promising approach for self-healing coatings is the encapsulation of liquid healing agents where the quick release of healing agents without any external input and good aesthetic results are very interesting properties. In 2001, White et al. [31] was the first to show a healing process of an epoxy composite in which embedded living polymerization (ring opening methathesis polymerization, ROMP) catalyst and an encapsulated dicyclopentadiene (DCPD) monomer reacted after micro-cracks were induced mechanically. The composite recovered up to 75% of the original strength. The most extended approaches consist of a two-agent system (resin and cross-linker or catalyst). Three possibilities exist:

- Encapsulating resin and cross-linker or catalyst in a double capsule system. [32]
- Components are encapsulated separately in a double capsule system. [33]
- One component is encapsulated while the second one is dispersed in the coating. This is the most common approach. [34]

However, there are also several drawbacks to this approach that have to be taken into account. Unfortunately, this approach only offers a single healing event on a local spot. The possibility exists that due to the dispersion of capsules in the coating that this could have a negative effect on the performance of the coating. A third drawback is that when the crack is filled, a depletion zone is left behind resulting in a possible degradation of the mechanical properties of the coating. Also the volume of the damage that can be healed is limited to the capsule volume and the volume fraction of the capsules and therefore a complete healing of the coating will not easily be reached. The final and main drawback is that for a two-component system, the two agents have to be in each other's proximity and have to be in stoichiometric ratios in order to react. [3]

Therefore, a system that uses a single healing agent that can react with components from the environment would lead to a more stable and guaranteed healing. Also the cost of these coatings would be less than the two-agent system as the use of a catalyst can be avoided. This approach showed already some interesting results, for example the encapsulation of tung oil for the protection of steel panels [35] [36] showed interesting corrosion protection behaviour. [3]

4. Approach in this work

With all the above knowledge in mind, the approach in this work is to further investigate *a single agent system that will "flow" when damage has occurred*. Healing agents that are encapsulated in a polyurethane shell are dispersed in a single layer PU coating. The main focus of the work will be on the encapsulation of IPDI, the synthesis of polyurethane coatings containing dispersed microcapsules and their ability to self-heal. However, other microcapsules are also synthesized.

4.1. Isophorone diisocyanate (IPDI)

One of the monomers that can have an autonomous polymerization reaction is the aliphatic diisocyanate, isophorone diisocyanate (IPDI). The molecular structure with the typical –NCO functionality is given in Figure 7. Diisocyanates have the potential to react with water at room temperature, as shown in Figure 6, to form an amine and CO_2 and this amine further reacts with IPDI to form polyurea and can therefore be used in a catalyst-free self-healing system. IPDI undergoes the following reactions:

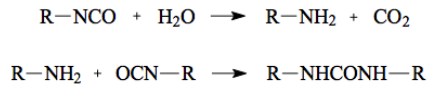

Figure 6: Reaction of IPDI with water. [14]

The dispersion of these capsules is best done in a PU coating to fully optimize the compatibility between the capsules, the healing agent and the coating matrix.

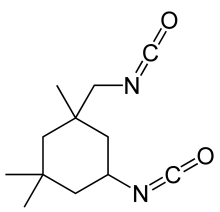

Figure 7: Isophorone diisocyanate (IPDI). [37]

Compatibility can be understood as the wetting of the matrix on the shell material of the capsules and this is the potential to form covalent bonds between both. Also the HA has to have a good wetting on the matrix coating so that it can flow in a defect and form bonds with the matrix in order to heal the defect.

In the past, the encapsulation of isocyanates was limited to the solid state or blocked form, which is not so suited for self-healing. [38][39] But since recently, it is possible to encapsulate liquid diisocyanates. Only a couple of articles have appeared on the encapsulation of liquid diisocyanates by a oil-in-water emulsification polymerization and even less on the use of these capsules in a self-healing coating [40-44], which makes it an ideal topic for further investigation.

4.2. Unsaturated fatty acids

Other types of healing agents are the unsaturated fatty acids. [4] In this work an unsaturated fatty acid "FD-2" of which the exact chemical composition is unknown, which is provided by the company Toseda, is encapsulated in two types of capsules. These fatty acids react with oxygen from the atmosphere and polymerize as shown in Figure 8. Unsaturated fatty acids undergo the following reactions:

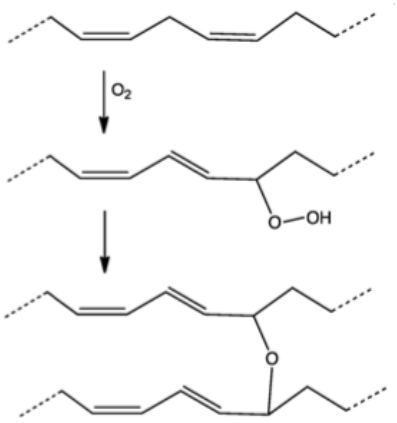

Figure 8: Reaction of unsaturated fatty acids with oxygen. [14]

Unsaturated fatty acids are suited as healing agents in alkyd coatings. However, because the main focus of this work is on the dispersion of microcapsules containing IPDI in PU coatings, no implementation of encapsulated unsaturated fatty acid "FD-2" in alkyd coatings is done in this work.

5. Techniques

This part aims to explain the principles of the techniques used in this thesis. A theoretical explanation will give a clarification of the advantages and disadvantages of each technique.

5.1. Fourier Transform Infrared Spectroscopy (FTIR)

Infrared light ranges from 12800 – 10 cm^{-1} and can be divided into the near-infrared region (12800 - 4000 cm^{-1}), mid-infrared region (4000 - 400 cm^{-1}) and far-infrared region (200 - 10 cm^{-1}). FTIR spectrometers are commonly used in chemistry because it is possible with this technique to get information on the structures of molecules. The common used region of the IR-spectrum by this technique is the mid-infrared region (4000 – 400 cm^{-1}) because the absorption region of most compounds, both organic and inorganic, is within this range. [45]

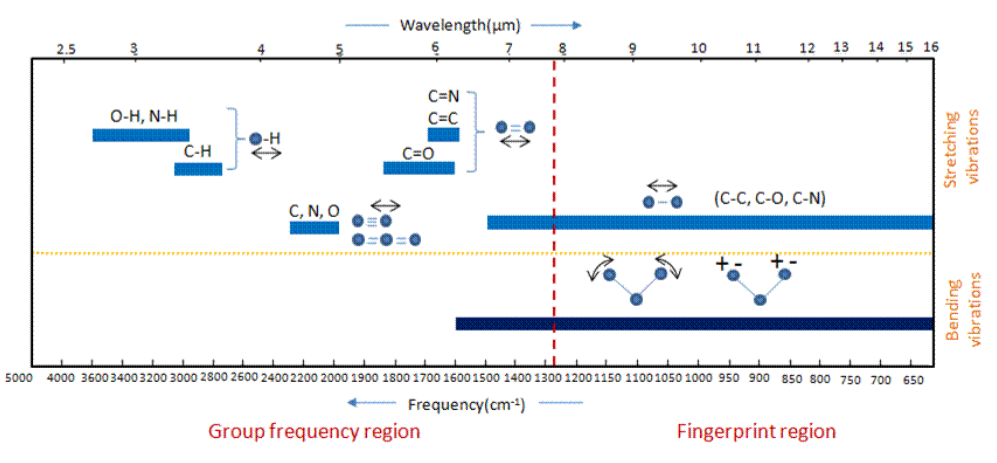

Figure 9: Group frequency and fingerprint region of the mid-infrared spectrum. [46]

Spectroscopy is defined as the interaction between light and mater. In an FTIR spectrometer, samples are exposed to infrared light and the molecules of the sample will selectively absorb radiation of specific wavelengths that are characteristic for the molecule. This absorption of radiation leads to a change of dipole moment of the molecules, by different vibration modes of the molecule. It is important to understand that only those bonds with vibrations that can show a change in dipole moment can absorb infrared radiation and these are called IR-active bonds. These IR-active bonds will show up in the spectrum, while the non-active bonds will not be seen. The energies associated with vibrations of atoms in a molecule with respect to one another are quantized and after absorption of light, the vibrational energy levels of the sample molecules transfer from the ground state to the excited state. The vibrational energy gap determines the frequency of the absorption peaks and the change of dipole moment as well as the possibility of the transition of energy levels determines the intensity of the peaks. When analysing the infrared spectrum or molecular vibration spectrum, it can be divided into a functional group frequency region (4000 – 1200 cm^{-1}) that helps identifying the structure of the molecule and the fingerprint region (1200 – 400 cm^{-1}) that is used for compound identification as is illustrated in Figure 9. [45]

5.2. Thermal analysis

5.2.1. Thermogravimetric analysis (TGA)

Thermogravimetric analysis is the measurement of weight changes of a system as a function of increasing temperature or time as the sample is subjected to a specific temperature program in a controlled atmosphere. A TGA device consists of a sample crucible, which is supported by a precision balance. This crucible is surrounded by a furnace and can thus be heated or cooled during the experiment while the mass is monitored. Purge gas flows over the sample and exits through an exhaust; mostly air or an inert gas (Nitrogen, Helium or Argon). [47]

With this technique, the thermal stability of a sample can be evaluated and this gives an indication of the temperature range in which the material can be used. The result of a TGA measurement also gives a range in which it is suitable to perform calorimetric measurements (DSC). Besides the thermal stability, the amount of volatile components can be determined. A step in a TGA curve during the heating of the sample indicates the mass loss of the sample due to for example the evaporation of water. [47]

5.2.2. Differential Scanning Calorimetry (DSC)

Differential scanning calorimetry gives information on the heat flow as a function of temperature. Information on the heat capacity as well as the thermal transitions of the sample is provided. Two classes of DSC instruments exists that both have a big difference in design and operation. The first class is the power-compensated DSC, where a sample crucible and a reference crucible are heated or cooled separately at a controlled rate. Their temperature is recorded and the differential heat input to the sample and the reference to keep both at the same temperature is monitored. The second class is the heat-flux DSC, where a single cell is used. The sample and the reference are heated or cooled at a controlled rate in this single cell and their temperature difference is measured. In Figure 10, a schematic representation of both classes is shown.

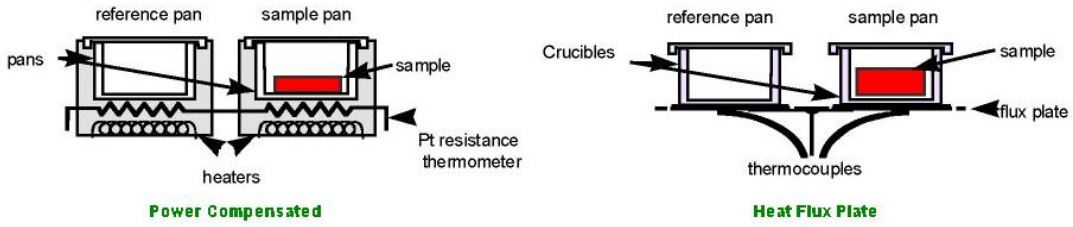

Figure 10: Schematic diagrams of a Power Compensation DSC (left) and a Heat Flux DSC (right). [48]

The heat flux of the sample is proportional to the temperature difference between the reference and the sample and can be expressed as follows:

$$\frac{dq}{dt} = K.\Delta T \tag{3}$$

With:

$$\frac{dq}{dt} = The\ sample\ heat\ flow\ per\ unit\ mass\ \left(\frac{W}{kg}\right)$$

$$\Delta T = Temperature\ difference\ between\ reference\ and\ sample\ crucible\ (K)$$

$$K = Instrument\ calibration\ factor\ (\frac{W}{K.kg})$$

This expression can also be represented as follows:

$$\frac{dq}{dt} = C_p(T).(\frac{dT}{dt}) + f(T,t) \quad (4)$$

In this equation the material parameters of the sample are used to express the general equation for the heat flow. Heat flow is expressed as a function of the heat capacity (C_p), the heating rate (dT/dt) and a term that is a function of the transformation of the sample. This term is dependent on the temperature (T) and also contains kinetic information; therefore it is also time dependent (t).

5.2.3. Thermal activity monitor (TAM)

Thermal activity monitor or TAM is an ultra-sensitive heat flow measurement that is complementary to DSC. Because all chemical processes consist of either heat production or heat consumption, this microcalorimeter can be used for studying the thermal activity of reactions with relatively small enthalpies. Heat, heat flow and heat capacity of a sample can be measured with a high sensitivity (<1 μW) and a long-term stability, thanks to a mineral oil bath. This device allows doing isothermal experiments (dT/dt = 0) over a period of several hours to one month. [49]

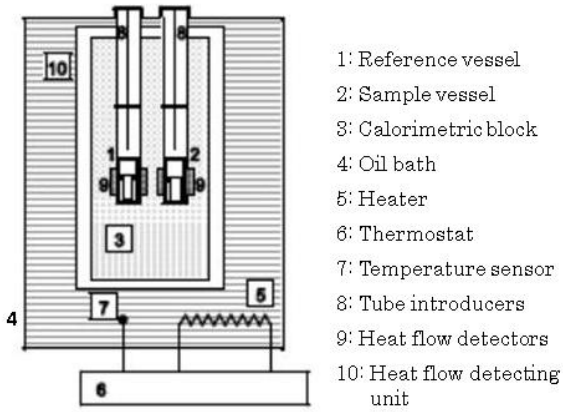

Figure 11: Schematic representation of a TAM calorimeter [50]

The liquid oil thermostat maintains at a constant temperature and any heat that is produced or consumed by the sample is continuously measured. Figure 12 shows an example of an isothermal TAM measurement showing the crystallization kinetics of polycaprolactone at different temperatures. It can be seen from the figure that the heat flow can be monitored up to one month because of the stable baseline.

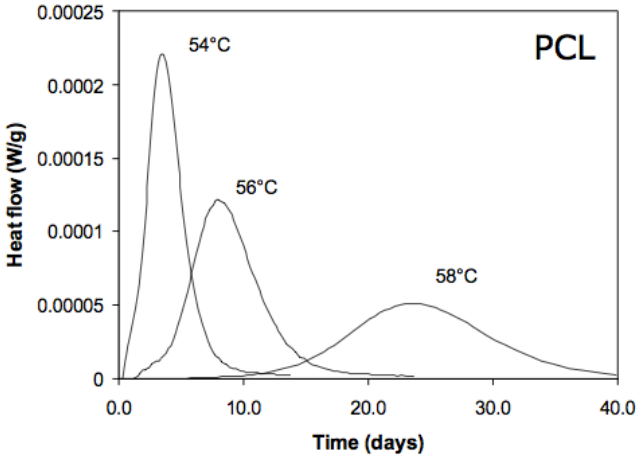

Figure 12: Isothermal TAM measurement showing crystallization kinetics of polycaprolactone at different temperatures. [51]

5.3. Electrochemical Impedance Spectroscopy (EIS)

This electrochemical method is used to provide information on corrosion mechanisms and on the effectiveness of corrosion control methods such as inhibitors and coatings. A small AC voltage perturbation (10 – 20 mV) is imposed on the electrochemical system in a broad frequency range (1 mHz – 100 kHz). The response current is measured as a function of the frequency and as such information on the frequency evolution of the impedance is obtained. The impedance Z is the proportionality factor between the imposed voltage perturbation E and the response current density i. [52]

$$Z(\omega) = \frac{E(\omega)}{i(\omega)} = \frac{E_0 \sin(\omega t)}{i_0 \sin(\omega t + \theta)} \tag{5}$$

$$\theta = arctan \frac{Z_{im}}{Z_{re}} \tag{6}$$

The different processes that can occur in an electrochemical system have different time constants and will thus be seen in different frequency regions. For example, when looking at organic coatings in a corrosive electrolyte, it is seen that the high frequency part of the spectrum is usually related to electrolyte resistance whereas the mid-to-low frequency part provides information on the barrier protection of the coating. The coating resistance is found at lower frequencies and the corrosion processes at the lowest frequencies. The information provided by EIS is commonly plotted in two different types of plots: the Nyquist plot and the Bode plot. The Nyquist plot represents the imaginary impedance (Z_{im}) as a function of the real impedance (Z_{re}) whereas the Bode plots represent the modulus of the impedance (|Z|) and the phase angle (θ) as a function of the frequency ($f = \omega/2\pi$). [9]

The systems can be modelled by an equivalent electrochemical circuit (EEC). This method is used for example to model coated metal surfaces in solution as is shown in Figure 13.

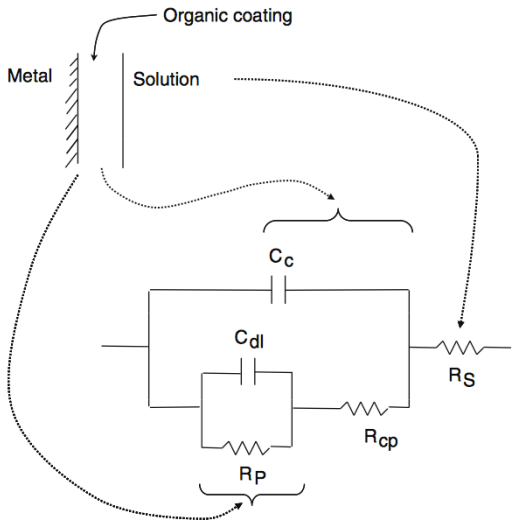

Figure 13: EEC for an organic coating on a metal substrate. [52]

The components of this EEC symbolize the coating capacitance (C_c) the capacitance of the double-layer at the metal-solution interface (C_{dl}), the polarization resistance of the metal (R_p), the pore resistance of the coating (R_{cp}) and the electrolyte solution resistance (R_s). [52]

The most interesting component is the pore resistance of the coating (R_{cp}) as it gives particular information on the degradation of the protective properties of the coating. This information can be used to rate and compare the quality of coatings and the corrosion behaviour. When looking at a calculated Bode plot (Figure 14), this information can be found at low frequencies where the impedance has a value that corresponds to $R_p+R_{cp}+R_s$. [52]

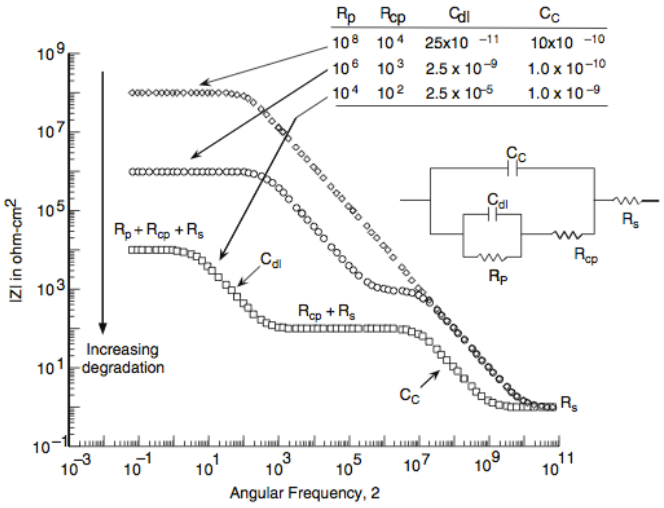

Figure 14: Calculated Bode plots for the EEC in Figure 13 for various input parameters. R in Ω and C in F/cm². [52]

In this work, EIS is used to investigate the corrosion resistance of the produced coatings in order to compare them and to determine whether an autonomous self-healing capability has occurred after damage was inflicted.

5.4. Surface analysis techniques

5.4.1. Optical Microscopy (OM)

An optical microscope (OM) uses visible light and optical lenses to magnify images of small samples. This device is often combined with a light-sensitive camera to capture an image. Although this device can provide a magnified image of the sample and the sample can be analysed non-destructively, several disadvantages have to be considered. One of them is that the resolution of the OM is rather limited (0,4 µm – 0,7 µm) due to the wavelength of visible light. Because of interference of the light waves, optical diffraction makes the image blurry. A microscope is characterized by its resolving power, which is the ability to distinguish two closely spaced items at the highest magnification. When a higher magnification and resolution is required, the limitations of the diffraction limit of visible light have to be avoided. This can be done using an electron beam (e.g. scanning electron microscope) or a mechanical probe (e.g. atomic force microscope). An image with a much higher magnification and resolution is achieved.

5.4.2. Scanning Electron Microscopy (SEM)

A scanning electron microscope or SEM bombards a sample with a focused electron beam and as a result of this bombardment, several signals that contain information about the sample are produced. In order for the electron beam to reach the sample without deflection or decrease in kinetic energy it may not collide with other particles on its way, therefore this device operates under high vacuum. When the electrons that are accelerated by a large potential collide with the sample, they penetrate into the material and interact with the sample's atoms at or near the surface of the sample. This interaction consists of a reflection, absorption or a transmission of the (primary) electrons. The types of signals produced include secondary electrons (SE), back scattered electrons (BSE), Auger electrons, cathodoluminescence, secondary fluorescence and characteristic X-rays. Depending on which beam is considered information on the surface topography or surface composition is obtained. [53]

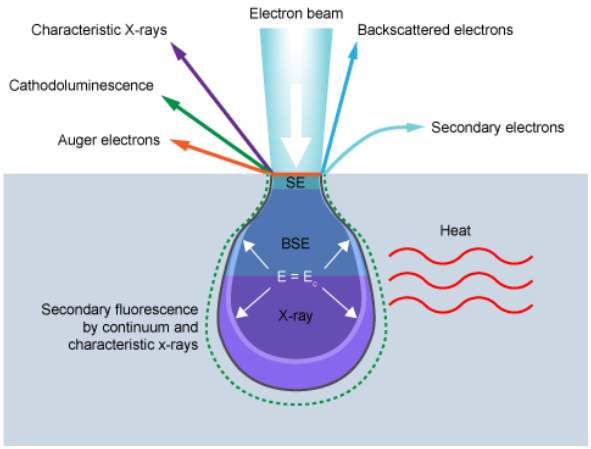

Figure 15: Interaction volume of a focused electron beam on a sample. [54]

In Figure 15 the interaction volume of the focused electron beam can be seen. This volume can range from less than 100 nm to 5 µm, depending on the atomic number of the sample and the energy of the beam. Although secondary and

Auger electrons are produced throughout the interaction volume, they have very low energies and can only escape from a thin layer near the sample's surface. This is similar for soft X-rays (< 5-10 keV) that are absorbed easily. Hard X-rays (> 5-10 keV) will be able to escape from the surface region of the interaction volume. [53]

It is important that the sample's surface is conductive to prevent having a charge build-up that can cause divergence of the electron beam and damage of the sample. The most standard setup of SEM and the one that is used in this work is the use of the secondary electron imaging (SEI) to produce high-resolution images of the surface of the sample. Because only the secondary electrons from the top layer of the surface can escape from the sample and are detected, a lateral resolution of several nanometres is achieved. These images have a three-dimensional appearance and are of great interest understanding the surface structure of a sample. [53]

Next to the conventional SEM, a field emission SEM or FE SEM is used to take images of the coatings. The difference between both is the way the electron beam is produced. In a conventional SEM thermionic emitters like tungsten or lanthanum hexaboride filaments do this, where for FE SEM the electron beam is produced by a field emission gun that creates a more coherent beam with a much smaller diameter resulting in a much higher spatial resolution and an increased emitter life. This results in a higher cost than for a conventional SEM. [53]

5.4.3. Atomic Force Microscopy (AFM)

An atomic force microscope is a type of scanning probe microscope that has a nanometer resolution. In Figure 16 the working principle of an AFM is shown. The key component of the AFM is the cantilever, which has at its end a small tip that acts as a probe to scan the surface of a sample. This tip is brought near or in contact with the surface of the sample and the resulting interatomic forces lead to a deflection of the cantilever. This deflection is measured by using a laser that reflects from the top of the cantilever and an image is created by raster scanning the surface. The benefit of AFM imaging is that the vertical height or depth of the sample's surface can be determined, making it a very suited way for observing particles or pits. Also this device does not require the sample to be conductive or to have a conductive layer, making it also suitable for the surface imaging of non-conductive samples. Unfortunately, there are also some limits. Amongst other, the scan speed and the scan area are rather limited and steep walls cannot be measured well, resulting in image artefacts. [55]

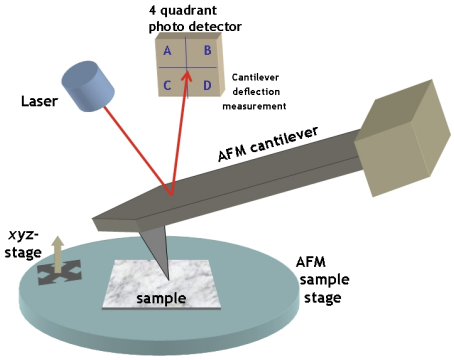

Figure 16: Schematic representation of the working principle of AFM. [56]

5.5. Techniques for coating application

5.5.1. Wire wound bar coater

The wire wound bar coater or rod is a stainless steel bar with a stainless steel wire wound around it. This rod is used to apply a substance in the liquid form on a substrate and this liquid cures to a solid coating. The area of the grooves between the wire determines the wet thickness of the coating, which is the theoretical thickness of the coating just after application. [57]

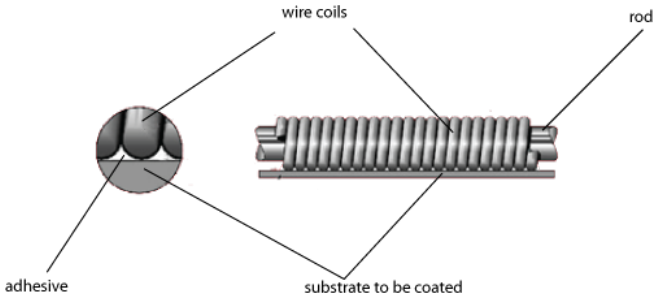

Figure 17: Representation of a wire coater. [58]

A wire coater gives a wet thickness. However, the actual wet thickness can deviate up to 90% of the theoretical wet thickness because the speed and pressure that is applied when using the wire coater manually, is inevitable altered each time. Therefore, it is more suited to use an automatic applicator when a high reproducibility of the coating thickness is acquired. The actual thickness or dry thickness is the thickness after solidification (e.g. by evaporation of solvent). [57]

5.5.2. Coating thickness gauge

The coating thickness gauge is able to measure the dry thickness of a non-conductive coating on a ferrous substrate such as steel. In order to do this, the device uses the principle of electromagnetic induction. The gauge consists of a rod that is wounded with a fine wire to produce an alternating magnetic field and a second coil that is used to detect the change in magnetic inductance, which can be directly related to the distance between the probe tip at the surface and the underlying substrate, and thereby the coating thickness is determined. [59]

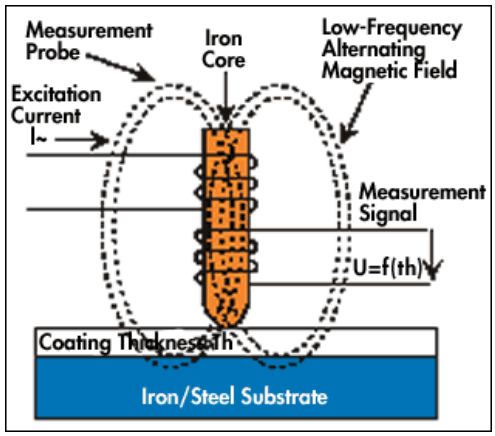

Figure 18: Schematic representation of the thickness gauge by the magnetic induction principle. [59]

III. Experimental

In this section the materials and the instruments and settings used in this work are specified. Part of the capsule synthesis was carried out at the company Toseda located in Pardubice, Czechoslovakia. The experiments were mainly carried out at the VUB unless otherwise mentioned.

1. Materials

1.1. Metal substrates

All the coatings were applied on the same type of substrates. These steel substrates were Q-panel standard test substrates acquired from Q-lab with following dimensions: 0,8 mm x 76 mm x 152 mm. Unless otherwise mentioned, the steel substrates were pre-treated to improve the adhesion of the applied coating. Prior to the pre-treatment, the substrates were cleaned with acetone and ethanol to remove contamination. The conversion solution used is a 1-3 wt% Granodine 1455T solution, with 0,5 g/L ammonium nitrate that acted as accelerator. The steel panels were submersed in this solution for 10 minutes. After immersion in the conversion solution, the substrates were cleaned with water or acetone when otherwise mentioned.

1.2. Chemicals for capsule synthesis and coating production

Capsules were produced by means of interfacial polymerization in an oil-in-water emulsion. First a prepolymer was synthesized. The materials used for the production of the prepolymer were toluene diisocyanate (TDI) containing 80 % of toluene 2,4-diisocyanate and the remaining 20 % consisting of toluene 2,6-diisocyanate obtained from Alfa Aesar; cyclohexanone obtained from Alfa Aesar (purity >99%); and glycerol obtained from Merck (purity >98%). For some different types of microcapsules, another prepolymer was produced with a different polyol. These polyols were castor oil provided by Toseda or 1,4-butanediol obtained from Merck (purity >99%). To attain an emulsion, sodium dodecyl sulphate (SDS) obtained from Fluka Chemika (purity >96%) or Gum Arabic provided by Toseda were used as surfactant. The main product used to produce the microcapsules was the manufactured prepolymer diluted in a solution of cyclohexanone. The polyol chain extender used to produce the shell wall was mainly glycerol. However, castor oil and 1,4-butanediol were also used to produce microcapsules.

The main healing agent that was encapsulated was isophorone diisocyanates (IPDI) obtained from Alfa Aesar (purity >98%). Two other healing agents that were tried to encapsulate were hexamethylene diisocyanate (HDI) obtained from Alfa Aesar (purity >98%) and a fatty acid with the name “FD-2” that was provided by Toseda of which the chemical composition was unknown.

In this work, the produced capsules are described by a specific name to distinguish their type and way of production. The following structure is used:

XY-Z

With “X” being the polyol used to produce the prepolymer. “Y” is the isocyanate used to fabricate the prepolymer. In this work, only TDI is used for the prepolymer production so the letter “T” will represent this product. “Z” is the encapsulated healing agent. The main type of capsule that is used in this work is the GT-IPDI capsule. This is a capsule made from the prepolymer produced with glycerol and TDI and this capsule encapsulates IPDI.

The coatings were produced using the synthesised (glycerol and TDI based) prepolymer and glycerol as polyol chain extender. Finding the best synthesis procedure was part of the research and is presented in Chapter IV.

2. Instruments and methodology

2.1. Fourier Transform Infrared Spectroscopy (FTIR)

FTIR was used to chemically characterise various components of the self-healing system.
FTIR spectra were obtained of the pure components used to produce the prepolymer and the capsules. The fabricated prepolymers were examined to see whether they still have the –NCO functionality that is needed for the synthesis of microcapsules. Produced microcapsules containing a HA were compared with empty capsules of the same type. Finally, different types of microcapsules were compared to each other.

FTIR is performed with a Nicolet 6700 smart iTR spectrometer with a diamond crystal. The angle of incidence was 45°. The scanning was performed 32 times to reduce the noise with a resolution of 4 cm^{-1}. The spectra obtained were between 600 and 4000 cm^{-1}. An automatic baseline correction and ATR correction were applied on the obtained spectra.

2.2. Electrochemical Impedance Spectroscopy (EIS)

EIS was used to test the quality of the produced coatings and to test their ability to self-heal after the application of a defect.
A series of EIS measurements was performed on coatings with 0, 5, 10, 15 and 20 wt% of GT-IPDI capsules. Uncoated Q-steel panels, with and without pre-treatment, were used as reference. The coatings were tested before damage was induced, immediately after the application of a defect and after a certain time of immersion in water. The samples were blown by pressurized air to remove possible dust and contamination before each measurement. The EIS measurements were conducted using the Autolab PGSTAT100.
For each measurement the area that is exposed was limited to 1,13 cm^2 with the use of tape. The electrolyte was 500 ml of a 0,4 M Na_2SO_4-solution. The measurements were performed with a platinum grid as counter electrode (CE) and a KCl saturated Ag/AgCl-electrode as reference electrode (RE). The working electrode (WE) and the CE were placed approximately 3 cm away from each other and the RE was placed in between at a distance of approximately 2 cm from the WE and CE. Before each measurement was started, the sample was kept in the electrolyte solution for 10 minutes to stabilize the potential. The OCP was measured for 30 seconds before each measurement. Around this reference potential a single RMS sine wave potential of 10 mV was applied. 50 frequencies

between 10^6 to 10^{-2} Hz were scanned; each time 10 cycles were done. The software used for the acquisition of the measurements was Nova 1.9. The interpretation of the data was done with the software Zview.

2.3. Thermal analysis devices

2.3.1. Differential Scanning Calorimetry (DSC)

To investigate the glass transition temperature of the capsules, DSC measurements were performed.
These were done on a TA Instruments DSC Q2000 with nitrogen as purge gas at a flow rate of 25 ml/min. The mass of the samples was between 2-5 mg. The crucibles used were Tzero hermetic aluminium crucibles from TA Instruments. The temperature range for the DSC measurements varied from -80 °C to 200 °C. To go to temperatures of -150 °C a liquid nitrogen cooling system (LNCS) was used. The used heating/cooling rate was 10 °C/min.

2.3.2. Thermal Gravimetric Analysis (TGA)

To determine the thermal stability of the capsules and to determine whether there is HA encapsulated, Thermal gravimetric analysis (TGA) measurements were performed.
TGA was done on a TA Instruments TGA Q5000 with nitrogen as purge gas at a flow rate of 25 ml/min. These measurements were carried out in platinum crucibles and the sample mass was around 2 mg. The starting temperature was equilibrated at 60 °C and brought to 600 °C at a heating rate of 20 °C/min.

The software to acquire the data for both TGA and DSC was Thermal Advantage. The data interpretation was done with TA Universal Analysis.

2.3.3. Thermal Activity Monitor (TAM)

The relative reactivity of two diisocyanates (HDI and IPDI) with water from the environment is evaluated by means of TAM measurements.
TA Instruments Thermal Activity Monitor III (TAM III) was used. The TAM III was set at an isothermal temperature of 25 °C. The average relative humidity in Brussels is approximately 78 % [60]. By placing a saturated NaCl solution in the TAM vessel, a relative humidity of 75.29 ± 0.12 % was simulated. [61]

2.4. Microscopy

2.4.1. Scanning Electron Microscopy (SEM)

SEM analysis of the different produced capsules was done to determine the morphology, the diameter and the size distribution of the capsules.

The scanning electron microscope (SEM) used to analyse the synthesized microcapsules was a JEOL JSM-6400 with a tungsten filament. Secondary electron imaging was used to acquire micrographs. The primary electron beam was accelerated to 5 keV or 20 keV. The micrographs were taken at different magnifications, varying between 500x and 10000x. The working distance (WD) used was 15.0 mm. The surface morphology, the diameter of the capsules and their size distribution were examined; the dry powder was placed on carbon tape and pressurized air was used to blow away the capsules that did not stick to

the tape. Several coatings were analysed with a field emission scanning electron microscope (FE SEM). The device used was a JEOL JSM-7000F that offers a high spatial resolution. The working distance was set to 10 mm. The primary electron beam was accelerated to 10 keV and the micrographs were taken at a magnification between 100x – 75000x.
A small platinum/palladium layer of 1 nm was sputtered on top of the coatings to make their surface conductive.

2.4.2. Optical Microscopy (OM)

To get visual information of the applied scratches in the coatings an optical Leica MZ-125 microscope was used equipped with an Olympus UC30 camera. Images were taken with a magnification of 10x, 50x and 100x.

2.4.3. Atomic Force Microscopy (AFM)

Several coating surfaces were investigated locally around an induced defect with AFM.
The device used to do this was a Park AFM XE-100. This is done immediately after the application of a scratch and again after some time when the coating was immersed in water to let it heal. An image was made by using tapping mode to scan an area with a size of 40 by 40 µm. A scan rate of 0,4 Hz was used to obtain the images with a resolution of 256 by 256 pixels. The obtained results were investigated with the program XEI.

2.5. Coating application and thickness determination

The steel panels were pre-treated by immersion in Granodine 1455T solution for 10 minutes. After this titanium conversion step, the substrates were rinsed with water or acetone when otherwise mentioned. Finally, they were dried by pressurized air.

The coating formulations were prepared by mixing the prepolymer/ cyclohexanone mixture with the triol glycerol. The amount of polyol needed was calculated to achieve a stoichiometric ratio of 1 OH-functional group to 1,1 NCO-functional group. Capsules were added as a powder to this formulation in an amount to get coatings with 0, 5, 10, 15 and 20 wt% of capsules. The capsules were added to the mixture and the mixture was then placed in a sonification bath for 10 - 30 minutes. The capsules that were dispersed in the coating were GT-IPDI capsules.

The coatings were applied on the steel substrate with a wire coater. Two wire wound bar coaters with a theoretical wet thickness of 100 µm and 500 µm were used. The wire coaters were obtained from Elcometer. After the application, the coatings were left to dry for 24 hours at room temperature.
A coating thickness gauge was used to measure the resulting dry thickness after the evaporation of the cyclohexanone and the curing of the coating. The used gauge was a Dualscope MP20.

2.6. Scratch application

For EIS measurement, the scratches were applied on the sample by means of a pen with a sharp tip. For the AFM measurements, the defect was induced by means of a scalpel. It was tried to always make scratches with the same length.

Figure 19: Scalpel (below) used for scratching of the samples for AFM. Pen with sharp tip (above) used to make defects in samples for EIS.

IV. Results

1. Synthesis and characterization of microcapsules

1.1. Introduction

The method to prepare the different microcapsules in this work was based on the method described by D. Sandori et al. [40] in the article "Polyurethane microcapsules with glycerol as the polyol component for encapsulated self healing agent". The production of microcapsules consists of two main parts. First an isocyanate terminated polyurethane prepolymer is prepared by reacting with glycerol as polyol in a 3:1 molar ratio. This prepolymer is a system of monomers that has reacted to an intermediate molecular weight state and this product is capable of further polymerization because of its reactive –NCO terminal isocyanate groups. In the second step this prepolymer is used for the encapsulation of the HA by interfacial polymerization of the prepolymer with glycerol as the polyol chain extender, in an oil-in-water emulsion system. Interfacial polymerization is the creation of an emulsion in which the reaction takes place at the interface between the prepolymer dissolved in cyclohexanone (oil phase) and the polyol chain extender that is soluble in water (water phase).

The emulsion is created by addition of a surfactant above the critical micelle concentration (CMC) and in order to overcome the interfacial tension, energy needs to be supplied. This can be done by stirring or by sonication of the surfactant/water mixture. It was proven during the internship of Hilke Verbruggen at Toseda [14] that the capsule size is dependent on the applied way and speed of mixing as can be seen in Figure 20. When a dispersion mixing head was used to agitate the mixture at a speed of 2000 RPM, microcapsules with a size between 10 and 100 µm were produced. When the agitation speed is increased, even smaller microcapsules were obtained. For capsules of submicron size, ultrasound dispersion can be used. It should be possible to create even smaller capsules, nanocapsules in this case, by combining both the mechanical mixer and the ultrasound dispersion [62].

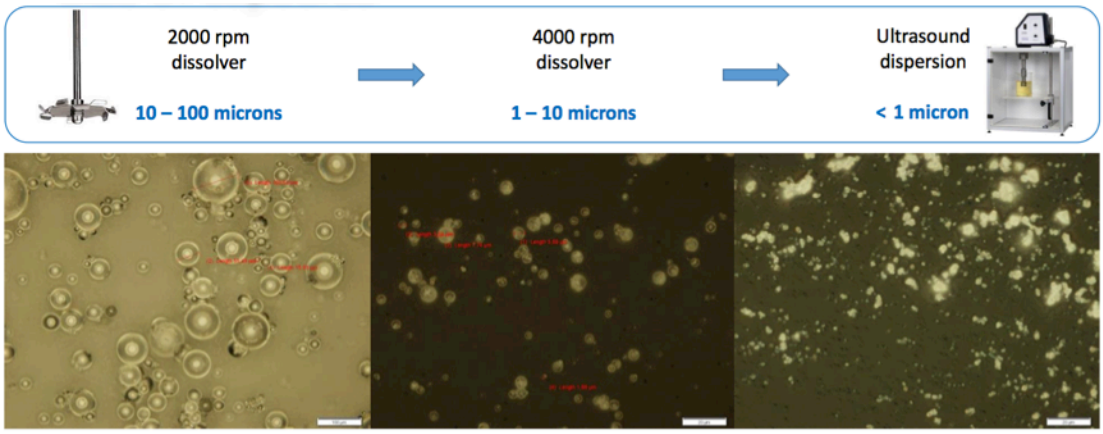

Figure 20: Dependence of the capsule size on the speed of agitation. [14]

Another important parameter of the microcapsules is their glass transition temperature (T_g) because of the relationship between the T_g and the Young's

modulus. It is important that the operating temperature is well below the T_g of the capsules in order for the capsules to undergo a brittle fracture when a defect occurs. It is also important that the capsules and the coating in which they are incorporated have a similar T_g, such that when a scratch is formed in the coating it also breaks the capsules while it propagates and that the crack does not propagate around the capsules. As coatings can be used in a range of different operating temperatures, it is of interest to be able to tune the T_g of the capsules likewise. At Toseda it was proven this could be achieved by changing the polyol component for the synthesis of the microcapsules. As such four types of microcapsules with a different T_g were produced and analyzed using DSC.

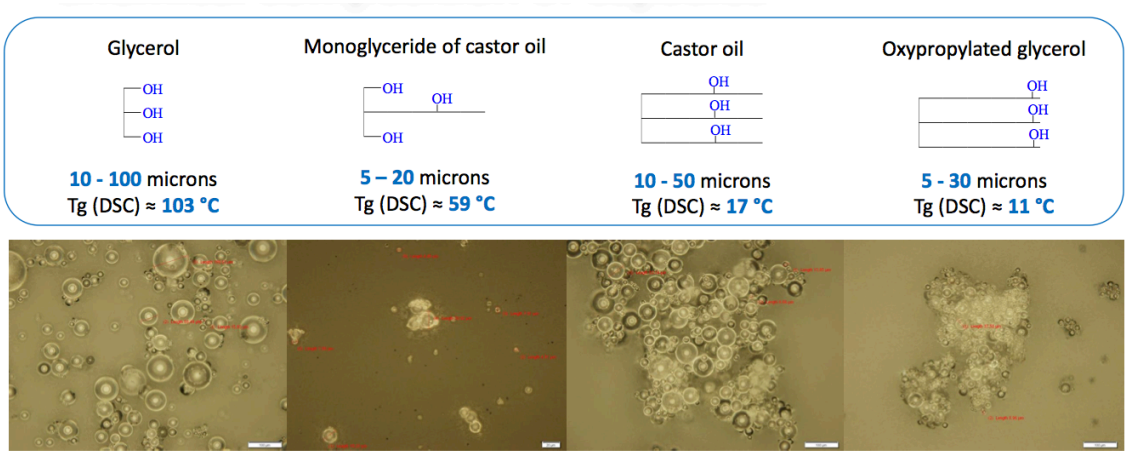

Figure 21: Microcapsules produced with different polyols resulting in a different T_g. [14]

The microcapsules were investigated at Toseda by performing DSC measurements. In Figure 22, the DSC measurement of a GT-IPDI capsule is shown. The measurement is performed with a heating rate of 20 °C/min and shows a glass transition temperature at 103 °C.

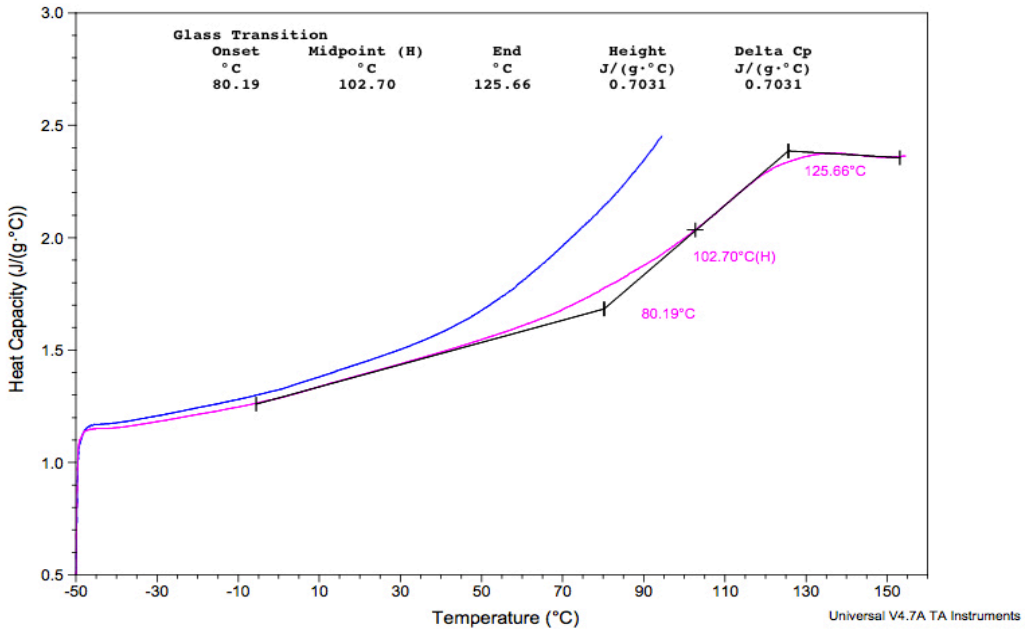

Figure 22: DSC measurement of GT-IPDI microcapsules, performed by Toseda. Heating rate 20 °C/min.

1.2. Synthesis of prepolymer

The synthesis of the prepolymer is the first step in the production of the microcapsules, as well as for the coating itself. As explained before, different polyols can be used as chain extender. In what follows, first the general synthesis procedure – using glycerol as polyol – will be explained, and then the different variations on this procedure will be clarified. 17 g TDI was dissolved in 50 g cyclohexanone in a 100 ml round-bottom flask. The mixture was heated to 80 °C in an oil bath, and stirred with a magnetic stirrer. 3 g of glycerol was added dropwise to the mixture with a Pasteur pipette. The flask was purged with nitrogen gas for one hour. Then the flask was sealed with Parafilm tape and the mixture was allowed to react further for 24 hours. The molar ratio of TDI to glycerol was 3:1 to keep the –NCO terminal groups in the prepolymer (see Figure 23). Different prepolymers of the GT-type were produced with a different amount of cyclohexanone in order to change the viscosity of the mixture, which had direct effects on the coating synthesis as will be mentioned later.

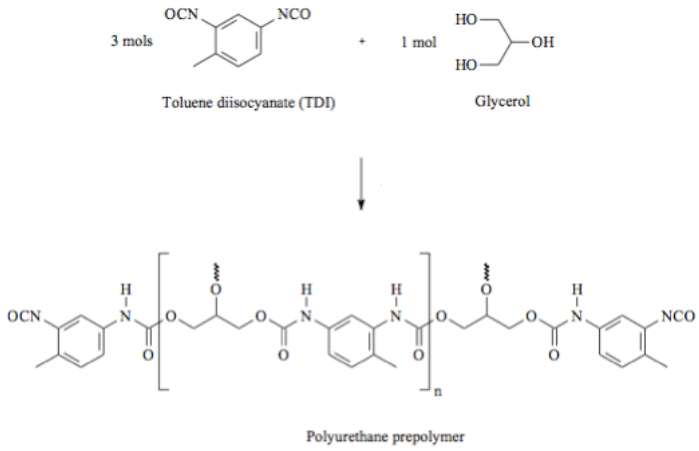

Figure 23: Reaction for the synthesis of GT prepolymer. [14]

When 1,4-butanediol was used as diol, 4,76 g of it was added dropwise to a mixture of 17 g TDI and 25 g cyclohexanone at 80 °C. This amount of diol was used to keep the same NCO:OH ratio. Just like the other type, the mixture was purged with N_2 for one hour and the flask was sealed with Parafilm to let the mixture further react for 24 hours.

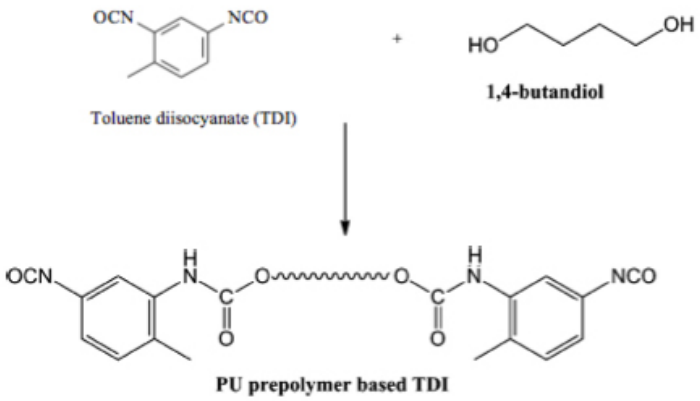

Figure 24: Reaction for the synthesis of BT prepolymer.

A final type of prepolymer was synthesized at Toseda using castor oil as polyol. 21,2 g TDI was dissolved in 61,7 g of cyclohexanone and this mixture was heated to 60 °C. Castor oil was added dropwise to the mixture and the flask was purged with N_2 for one hour. The mixture was then heated to 80 °C and then allowed to react for 4,5 hours. TDI and polyol reacted in a 2:1 NCO to OH group ratio.

After the production of each prepolymer, the solid content was determined. This solid content is the amount of prepolymer that is present in the prepolymer/cyclohexanone mixture. This was done by putting ca. 1 g of mixture for 30 minutes in an oven at 150 °C. After this time, the weight loss was determined to calculate the amount of evaporated cyclohexanone.

A list of produced prepolymer/cyclohexanone mixtures can be found in the Appendix.

1.3. FTIR results of produced prepolymer

To see if the prepolymer/cyclohexanone mixtures still have terminated NCO groups an FTIR analysis was performed on the three types of prepolymer that were produced.

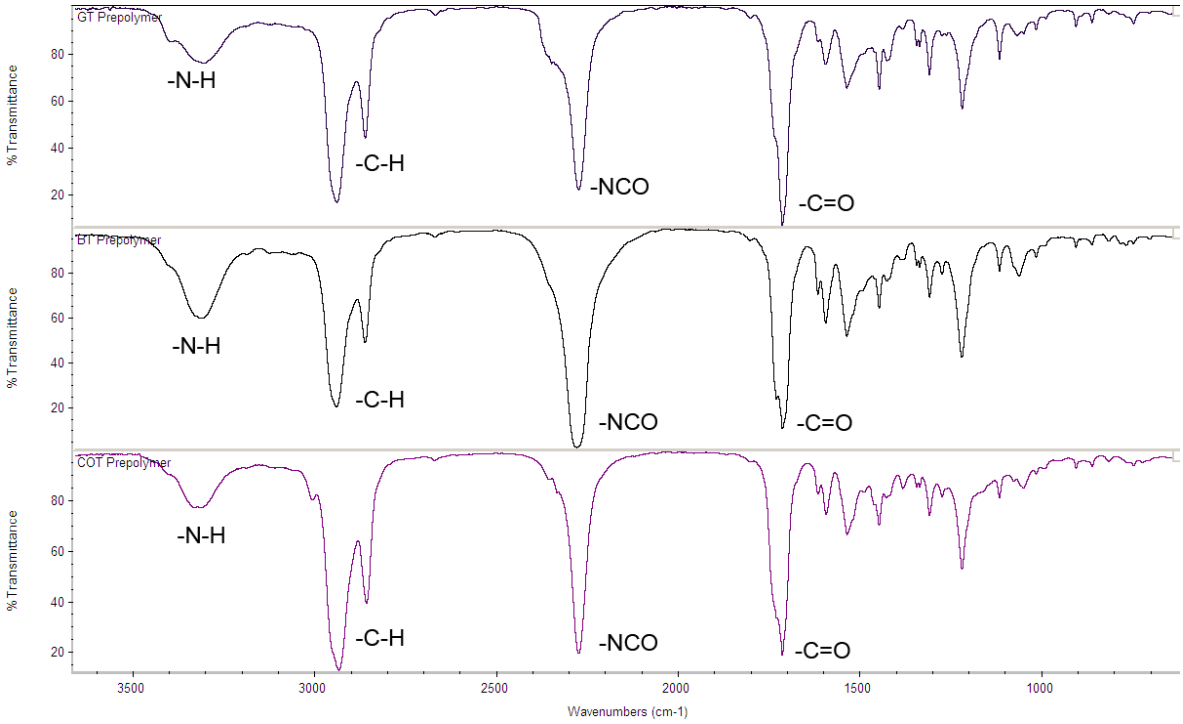

Figure 25: FTIR results of the prepolymer/cyclohexanone mixtures: GT prepolymer (top), BT prepolymer (mid) and COT prepolymer (bottom).

In the spectra of the prepolymer mixtures (Figure 25) the NCO stretching band is clearly visible at 2250 cm^{-1} for the three types of mixtures. The produced prepolymers still have unreacted isocyanate groups that can react with a polyol chain extender in the encapsulation step. The peak around 3400 – 3300 cm^{-1} can be allocated to the NH stretching group whereas the peak around 1540 – 1530 cm^{-1} can be related to the NH bending vibrations. The peak just above 1000 cm^{-1} can be related to the C-O-C band. These peaks confirm the formation of a urethane linkage.

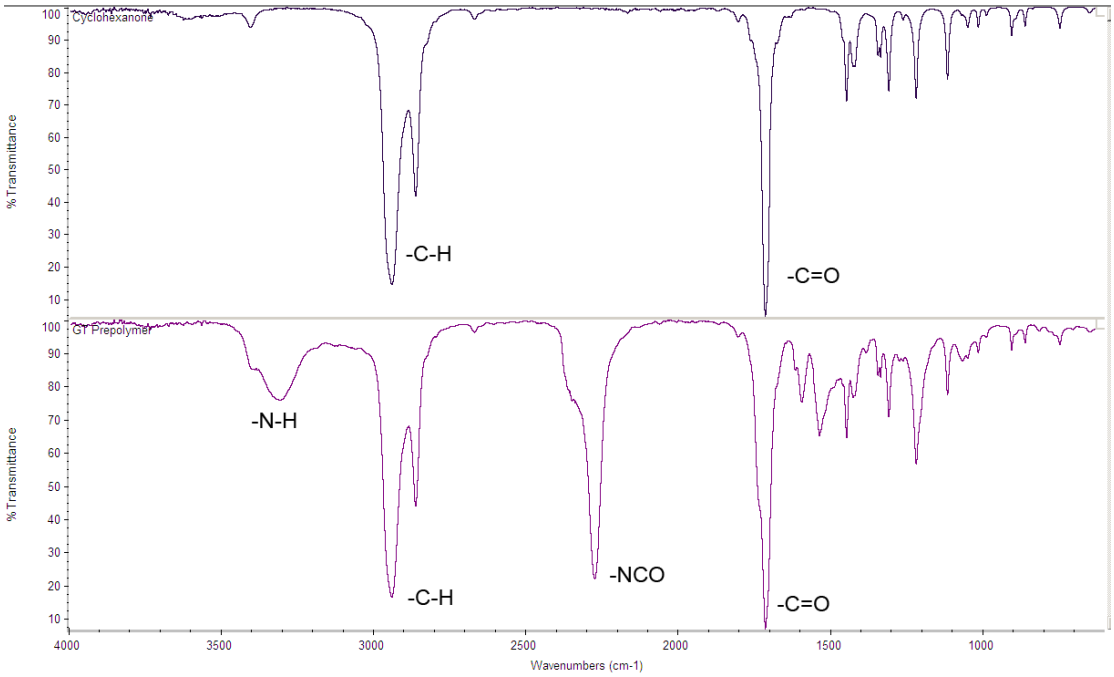

Figure 26: FTIR spectra for pure cyclohexanone (top) and GT prepolymer/cyclohexanone mixture (bottom).

By comparing the spectra of pure cyclohexanone and GT prepolymer/cyclohexanone mixture in Figure 26, it can be seen which peaks are related to cyclohexanone and which ones are related to the prepolymer. A typical peak due to C=O stretching around 1720 cm^{-1} is observed. Two medium-strong peaks are seen around 2950 and 2850 cm^{-1}, which are related to CH stretching vibrations.

1.4. Synthesis of different types of capsules

For the encapsulation of the healing agent, an oil-in-water emulsion was created with a surfactant. The PU capsules were created by an interfacial polymerization of the TDI based prepolymer and a polyol. This polyol, dissolved in the aqueous phase of the emulsion, acted as a chain extender for the formation of the shell wall and diffused into the oil phase droplet. This polyol reacted upon diffusion in the droplet with the TDI based prepolymer to form a PU layer and thus encapsulating the healing agent. This healing agent has to be soluble in the oil phase of the emulsion in order to be encapsulated. When the healing agent is IPDI, the polyol reacts with the more reactive TDI based prepolymer and not with the IPDI that thus gets encapsulated. The large difference in reactivity between an aliphatic (IPDI) and an aromatic (TDI) diisocyanate is exploited.

The main focus of this work is on the synthesis of GT-IPDI capsules that were produced as follows. At room temperature, 100 ml of water and 4,5 g of SDS were mixed in a 400 ml beaker for 30 minutes. The emulsion was agitated by sonication to obtain capsules with a small diameter. The amplitude of the sonicator was set to 50 % (30 W) and the pulse duration was 5 s with an interruption of 0,1 s. The mixture was placed in an ice bath to reduce the heating effect of the sonicator. The agitation lasted 1 hour in total.

Meanwhile, 2,9 g of healing agent IPDI was added to 2,9 g of prepolymer. This mixture was added slowly and dropwise to the SDS emulsion with a Pasteur pipette. After the addition of the oil phase, 0,4 g of glycerol dissolved in 5 ml of water was added slowly and dropwise. The mixture was allowed to further react for 45 minutes when it was cooled down to ambient temperature by addition of 100 ml of demineralized water. The suspension of microcapsules was than centrifuged at 10000 RPM for 30 minutes. Then the water is decanted and the microcapsules are rinsed again with demineralized water. Then the capsules were centrifuged again, this cycle was done for 5 times. Finally, this suspension was air dried for 24 hours in order to obtain a dry powder of microcapsules. A schematic representation of the complete synthesis of GT-IPDI microcapsules is shown in Figure 27, for the synthesis at Toseda the surfactant Gum Arabic was used instead of SDS.

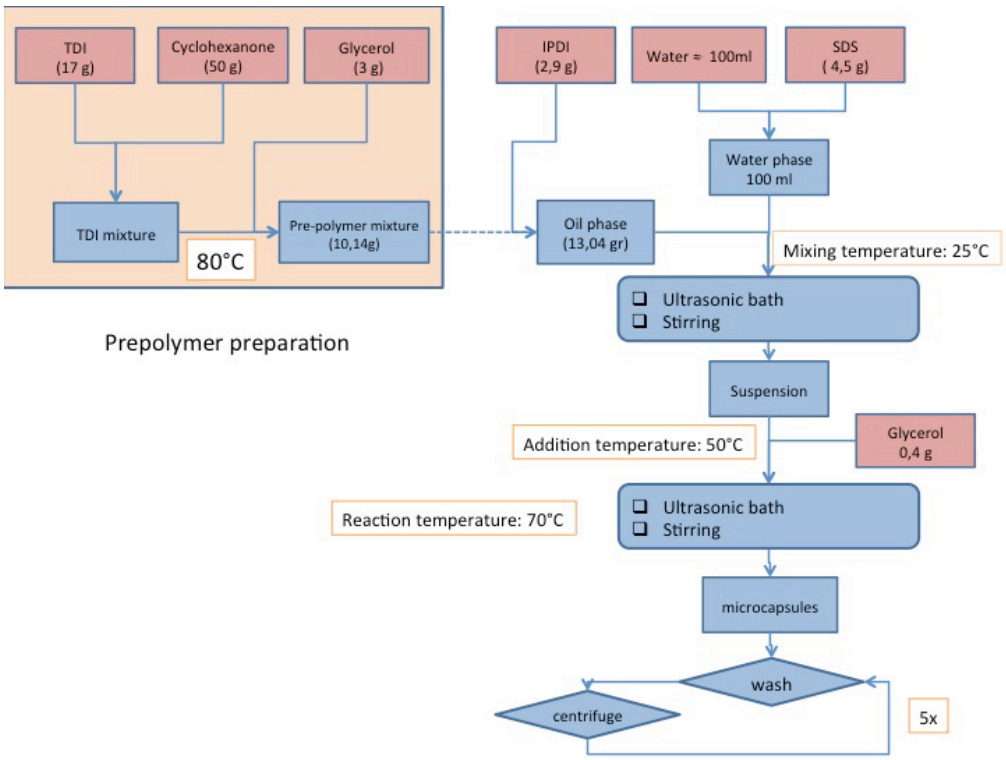

Figure 27: Schematic representation of the synthesis of GT microcapsules.

The synthesized capsules at Toseda were produced with a slightly different method. The Gum Arabic emulsion was agitated with a dispersion mixing head at 500 RPM. Just before the addition of the prepolymer-IPDI mixture, this speed was increased to 2000 RPM. The used temperature profile is represented in Figure 27.

The reaction that takes place between the PU prepolymer and the glycerol is shown in Figure 28.

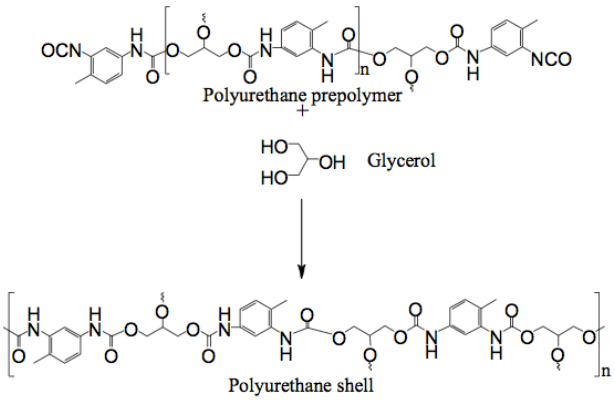

Figure 28: Reaction for the synthesis of GT microcapsules.

It was observed during the conduction of the experiments that sometime big yellow chunks were formed and less of the white powder (the microcapsules). It was even observed that when agitation was performed with a magnetic stirrer, only yellow chunks were formed till an agitation speed of 800 RPM. But above this agitation speed still yellow chunks but also powder was formed. When the agitation was performed with the sonicator, it seemed that less chunks were formed than when the agitation was done by magnetic stirring.

An important observation was that when using the dispersion mixing head mixer from Toseda, no chunks were observed at an agitation speed of 2000 RPM. However, an important difference between the capsules made at VUB and those made at Toseda was that the used surfactant was different. For the capsules made at Toseda, the surfactant was Gum Arabic while for those made at VUB the surfactant was SDS. For the future production of microcapsules, Gum Arabic should be tried as surfactant for the emulsification as it seems that the yields of the interfacial polymerization are better when Gum Arabic is used as surfactant. However, this is not proven to be solely or even at all the effect of the surfactant. It might also be due to the dispersion mixing head i.e. that by this stirring method more energy is added and that the emulsion is more stable. It must be kept in mind that the observations of the yellow chunks were visually observed and thus that they are rather subjective.

Other GT microcapsules with different healing agents were synthesized, and their method of production is very similar to the standard GT-IPDI type. First empty GT capsules (GT-Empty) were produced to compare both filled and empty capsules. These capsules were produced in exactly the same way as the procedure mentioned above, however the healing agent IPDI was not added to the oil phase. Note that 'empty capsule' is a somewhat misleading term as this does not mean that the capsules are void. It is assumed that they have a liquid core containing the solvent cyclohexanone.

A third type of GT capsules was prepared by encapsulating of the unsaturated fatty acid FD-2. These capsules were synthesized at Toseda and therefore the procedure slightly differs: Gum Arabic (4,5 g) was used as surfactant instead of SDS, and the agitation was done by a dispersion mixing head stirrer at 2000 RPM. For the same amount of prepolymer and polyol, 2,9 g of FD-2 was used.

By changing the polyol chain extender to the diol 1,4-butanediol a completely different type of microcapsules was synthesized. As already explained in the previous section, BT prepolymer mixture was produced to create this type of microcapsules. The same method as for the GT capsules was used to create BT capsules. The schematic representation of synthesis of BT capsules is shown in Figure 29.

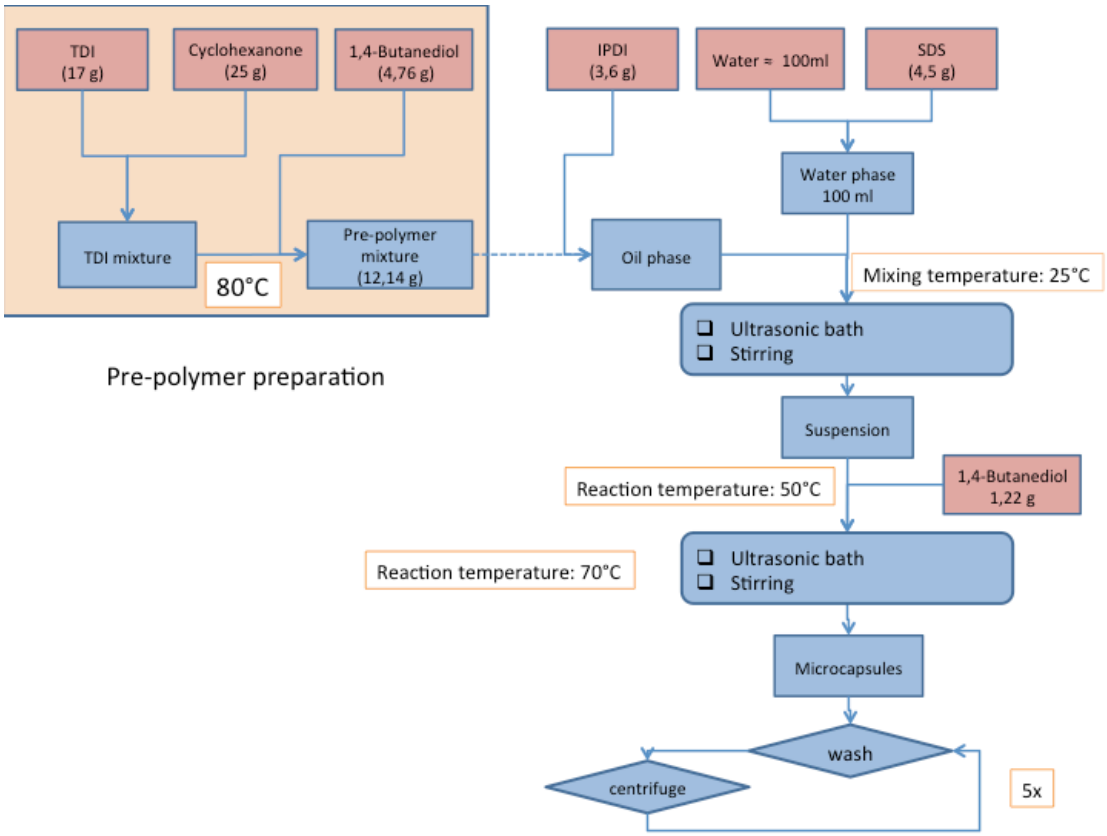

Figure 29: Schematic representation of the synthesis of BT microcapsules.

A third type of microcapsules is the COT microcapsules, which were synthesized with COT prepolymer mixture. Three types of COT microcapsules were synthesized: one without a healing agent (COT-Empty), one with 2,9 g IPDI added to the oil phase as healing agent (COT-IPDI), and one whereby 2,9 g FD-2 was encapsulated. All these types were produced at Toseda using a dispersion mixing head stirrer at 2000 RPM and 4,5 g Gum Arabic as surfactant.

A complete list of all the produced microcapsules can be found in the Appendix. Of all the produced capsules, only GT-IPDI capsules were incorporated in PU coatings as the focus of this work lies on this type of microcapsules.

1.5. Reactivity of the healing agents

The healing agent IPDI has to be able to react with water from the environment, without the use of catalysts. Therefore, the reactivity of IPDI in a humid environment was tested by performing a TAM experiment. Hexamethylene diisocyanate (HDI) – which is a more reactive aliphatic diisocyanate – was also tested for comparison. A constant relative humidity similar to the average relative humidity of Brussels was simulated in the TAM vessels by making use of a saturated salt solution.

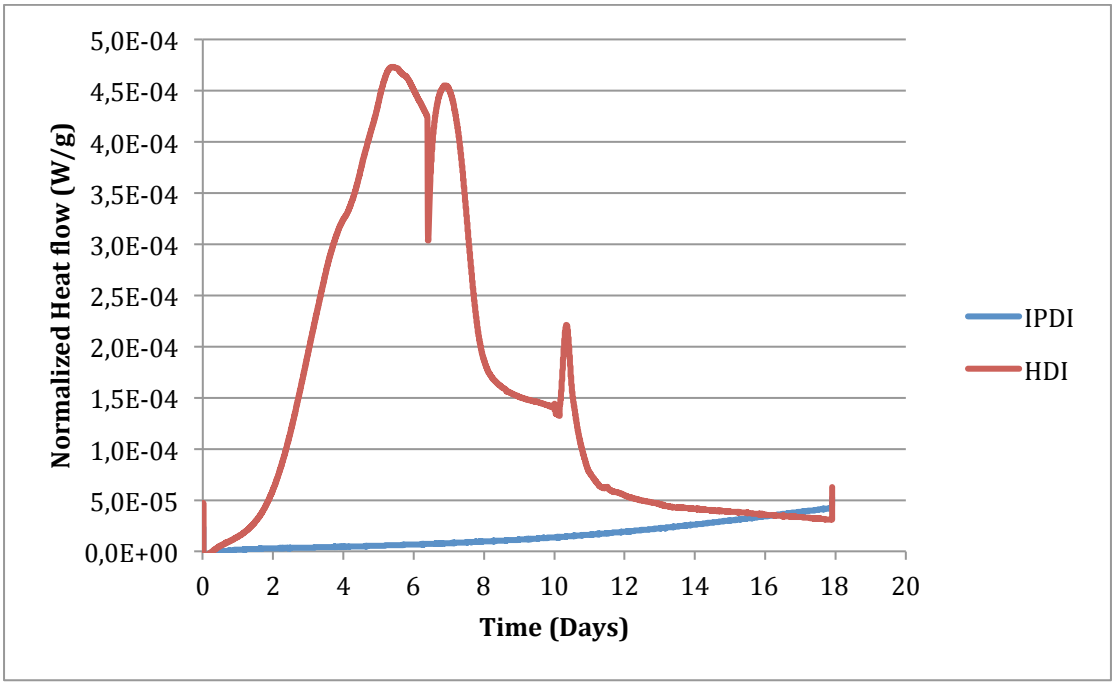

Figure 30: Reactivity of diisocyanates with water from the environment. Normalized heat flow (W/g) as a function of time (days). (Exo up)

Figure 30 shows the heat flow as a function of time of the reaction of two diisocyanates with water from the environment at 25 °C. The measurement duration was 18 days. The heat flow of HDI (red curve) increases after 2 days, while the heat flow of IPDI (blue curve) starts to increase very slowly after 8 days. This proves that HDI is much more reactive with water from the environment than IPDI. Therefore, it was also considered to encapsulate HDI as a healing agent. This would imply that when capsules with encapsulated HDI are incorporated in a coating, this coating might be able to heal faster a defect.

Given the above information, it was tried to encapsulate HDI using the GT prepolymer. Two types of GT-HDI capsules were tried to be made, one by mechanical mixing at 2000 RPM and one with sonication (using the same settings as previously mentioned). The same procedure as shown in Figure 27 was used, however the only difference was the addition of 2,9 g HDI (instead of 2,9 g of IPDI) in GT prepolymer/cyclohexanone mixture (oil phase).

It was visually observed that before the centrifuging step, a milky solution was synthesized for both the mechanical stirring and sonication procedure. This milky solution looked different than the previously made suspensions. Also

when the suspension was put on a shelf for the microcapsules to settle, no sediment was observed. This was an indication that something was different for this type of capsules.

1.6. FTIR results of the synthesized capsules

The synthesized capsules were analysed by means of FTIR spectroscopy. The different produced GT, BT and COT capsules with and without the healing agent IPDI were analysed and can be compared with their respective prepolymers. Also two types of GT-IPDI capsules that were produced by sonication and by mechanical stirring were compared with each other. The synthesized capsules with FD-2 were also analysed but the spectra are not presented in this work. Furthermore, the FTIR spectra of the powders that were obtained after centrifugation of the produced GT-HDI suspensions are presented.

The spectra of pure cyclohexanone and IPDI are shown in Figure 31 as it is assumed that a mixture of these two components is the liquid core of the GT-IPDI capsules. The NCO peak at 2250 cm^{-1} of IPDI has a rather odd shape because this is a very large peak and this peak was altered due to the performed corrections.

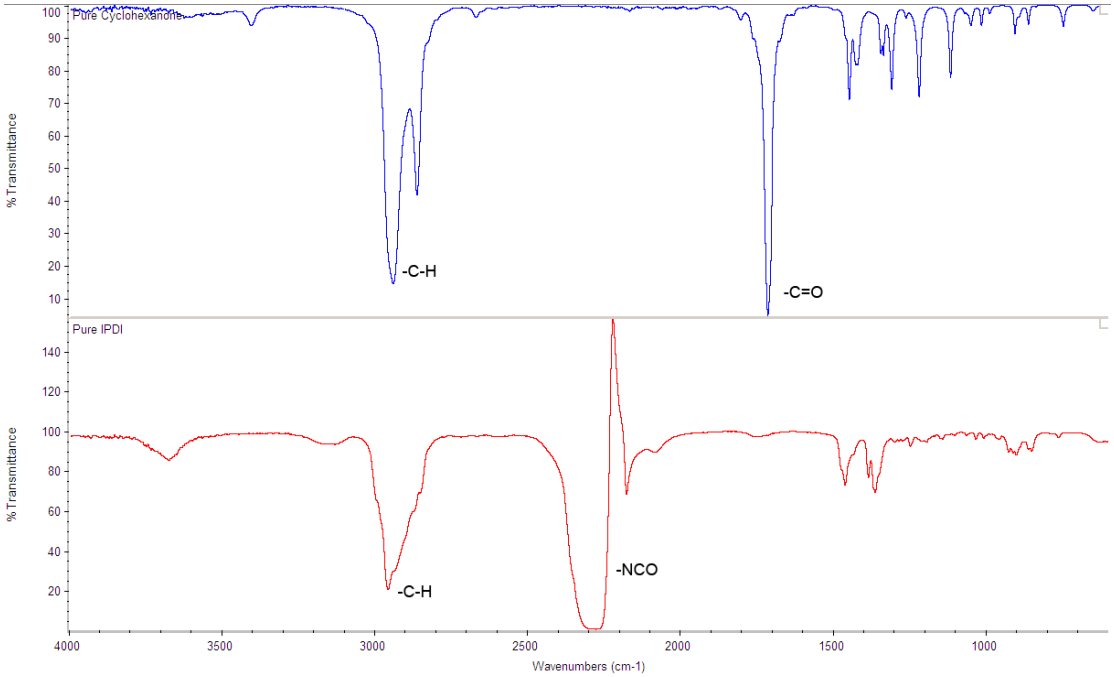

Figure 31: FTIR spectra of cyclohexanone (blue) and IPDI (red).

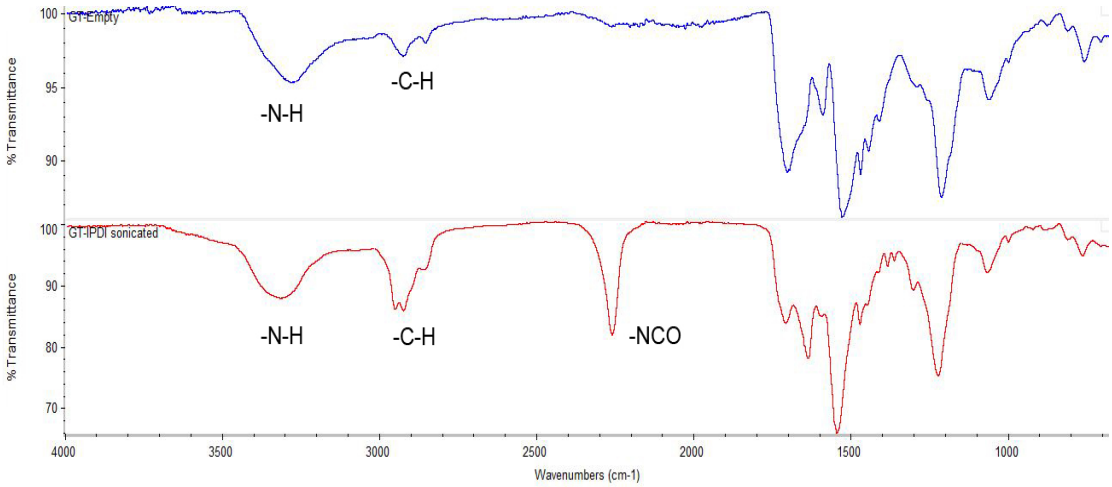

Figure 32: FTIR spectra of GT-Empty (blue) and GT-IPDI (red).

In Figure 32, the FTIR spectra of GT-Empty (blue) and GT-IPDI (red) are shown. An important observation that can be made is the absence of a –NCO peak at 2250 cm^{-1} for the microcapsules where no IPDI healing agent was added to the oil phase, whereas this peak is seen for the spectrum of GT-IPDI capsules. This indicates that there is IPDI in or on the outside of the latter microcapsules. However later observations indicate that here it can be concluded that the healing agent IPDI was successfully encapsulated in a PU shell.

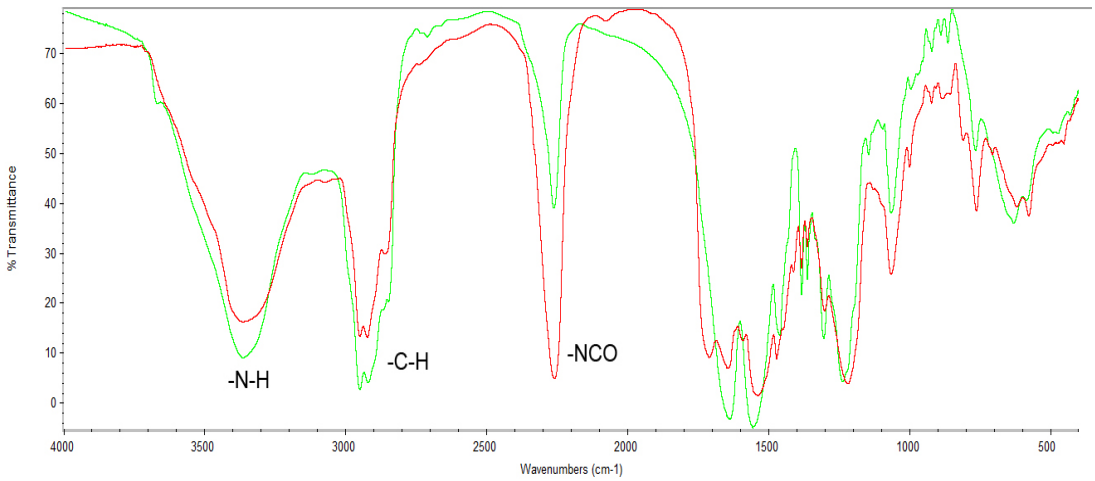

Figure 33: FTIR spectra of GT-IPDI produced by sonication (red) and by mechanically stirring (green).

By comparing the FTIR spectra of GT-IPDI capsules that are produced by sonication and by mechanically stirring (Figure 33), it can be seen that the –NCO peak is observed for both types of microcapsules. This is an indication that by both techniques microcapsules containing IPDI were produced. This also implies that the encapsulation was successful with both methods of agitation.

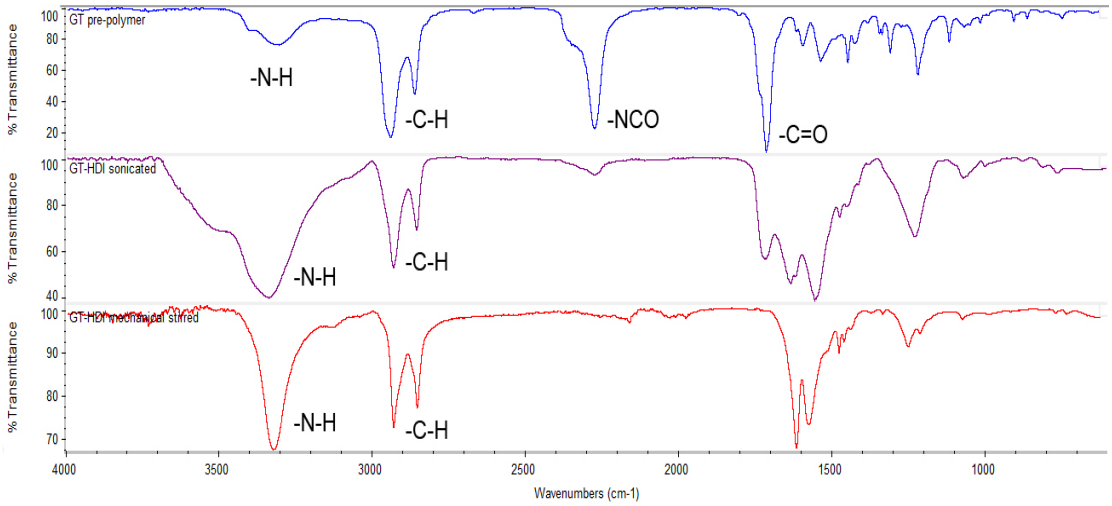

Figure 34: FTIR spectra of GT prepolymer (blue), GT-HDI sonicated (purple) and GT-HDI mechanically stirred (red).

When looking at the FTIR spectra of the GT-HDI powders, it is seen in Figure 34 that the –NCO peak is very small and even absent for the sonicated and the mechanically stirred microcapsules respectively. This is an indication that something was not the same as for the synthesized microcapsules containing IPDI.

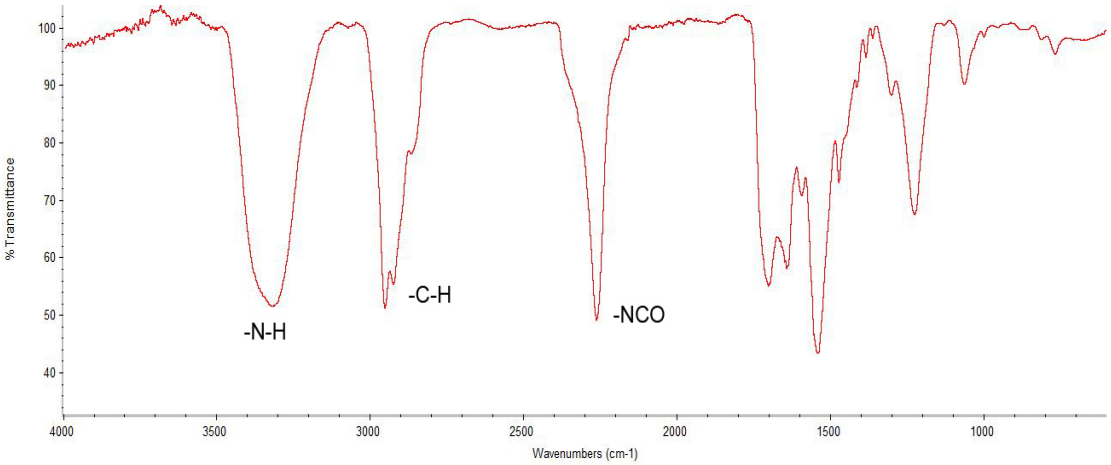

Figure 35: FTIR spectrum of BT-IPDI (red).

Figure 35 shows the FTIR spectrum of sonicated BT-IPDI (red). Following the same reasoning as for the GT-IPDI capsules and due to the similarity in the way of synthesis of the microcapsules the same conclusions can be made. The NCO peak at 2250 cm^{-1} is clearly seen, which is again an indication for the successful encapsulation of IPDI (if the same reasoning can be made).

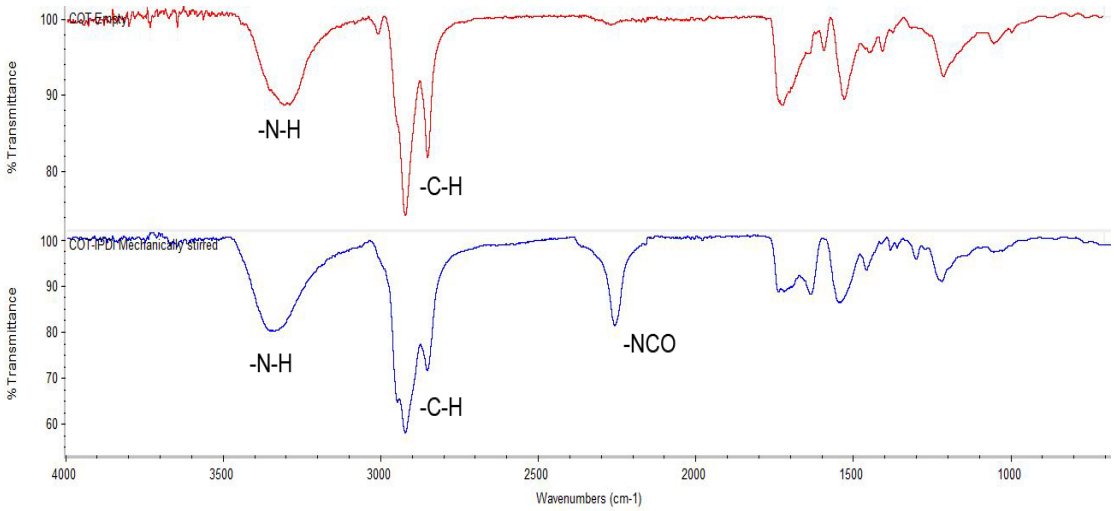

Figure 36: FTIR spectra of COT-Empty (red), COT-IPDI (blue).

In Figure 36, the FTIR spectra of microcapsules without healing agent (COT-Empty) and with the healing agent IPDI added to the oil phase during production (COT-IPDI) are shown. Again the same indications are there i.e. that the FTIR spectra of COT-IPDI contains a peak at 2250 cm^{-1}, the –NCO peak is visible whereas for the COT-Empty microcapsules, no peak is observed at this wavenumber.

1.7. SEM images of the synthesized capsules

The morphology of the different synthesized powders is analysed by SEM. Also the size and the size distribution of the capsules were observed. First two types of GT-Empty microcapsules are compared with each other; one produced by sonication and the other by mechanical stirring. These empty capsules were also crushed to try to determine the shell wall thickness of the microcapsules. A second method for trying to determine the shell wall thickness was by embedding the microcapsules into a resin and by polishing the resin surface. After this, two types of GT-IPDI are compared to each other; again one type by stirring and another one produced with sonication. Then BT-IPDI capsules (again produced by sonication and mechanical stirring are compared to each other as well as COT-Empty and COT-IPDI produced by mechanical stirring. Furthermore, micrographs of GT-HDI (sonicated and mechanically stirred) are analysed.

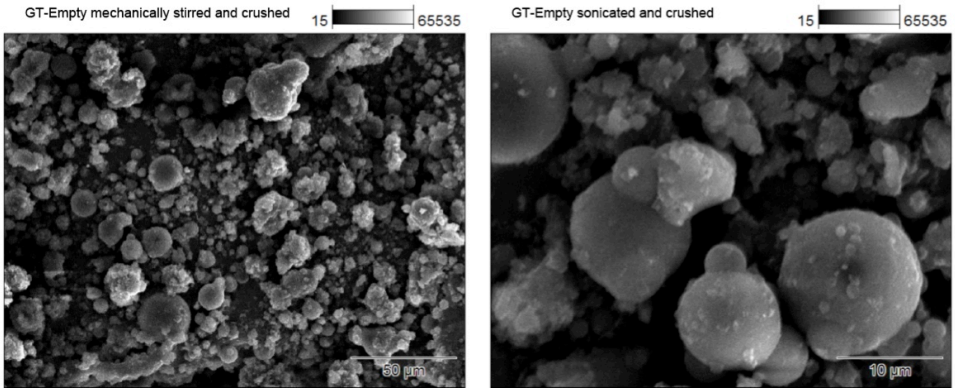

Figure 37: SEM images of GT-Empty mechanically stirred (20 keV; 500x; left) and GT-Empty sonicated (20 keV; 2500x; right).

When comparing both GT-Empty microcapsules, the first observation that can be made is that spherical microparticles have been formed. The mechanically stirred GT-Empty clearly had a larger size (1 – 30 µm) than the GT-Empty sonicated (500 nm – 1 µm) and in addition also a larger size distribution. Because of the mechanical crushing of the capsules, debris is seen in between the spherical capsules. Unfortunately, it was not possible to clearly detect a microcapsule shell wall to determine the thickness. By embedding the microcapsules in a resin a rather large microcapsule (200 µm) is observed, showing a shell wall thickness of around 10 µm (Figure 38). Unfortunately, it was not possible to find any smaller microcapsules.

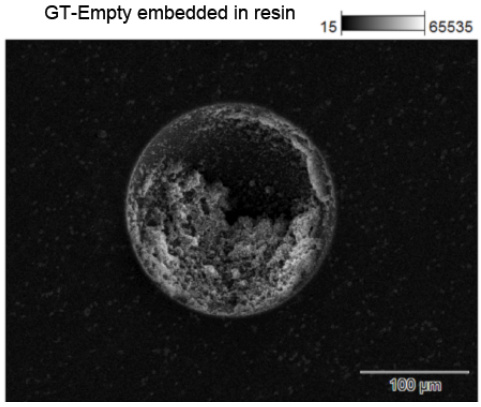

Figure 38: SEM image of a mechanically stirred GT-Empty microcapsule embedded in resin.

When comparing mechanically stirred and sonicated GT-IPDI microcapsules, some remarks have to be made. GT-IPDI sonicated was synthesized at VUB with surfactant SDS and the sonicator as agitation method. The main difference with the GT-IPDI mechanically stirred is that these capsules were produced at Toseda with Gum Arabic as surfactant and a dispersion mixing head at 2000 RPM as agitation method. Both types of capsules can be seen in Figure 39. Another remark is that for the mechanically stirred GT-IPDI capsules some charge build up was seen on the microcapsules when analysing them, although this had no severe consequences.

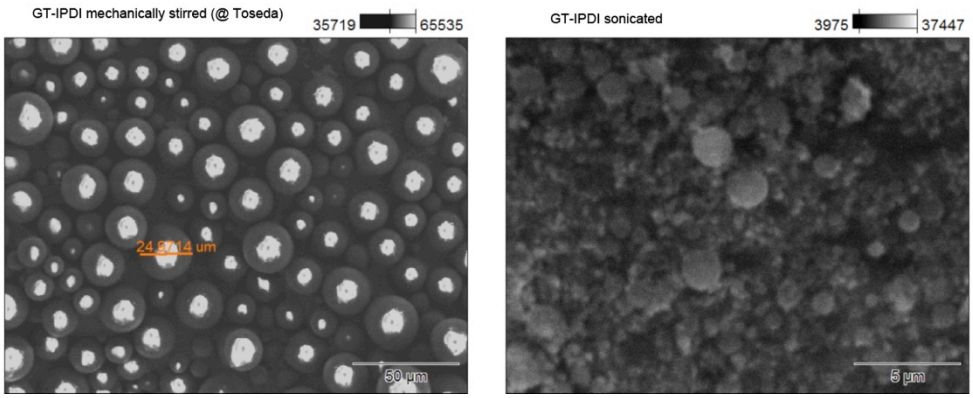

Figure 39: SEM images of GT-IPDI mechanically stirred (5 keV; 500x; left) and GT-IPDI sonicated (30 keV; 5000x; right).

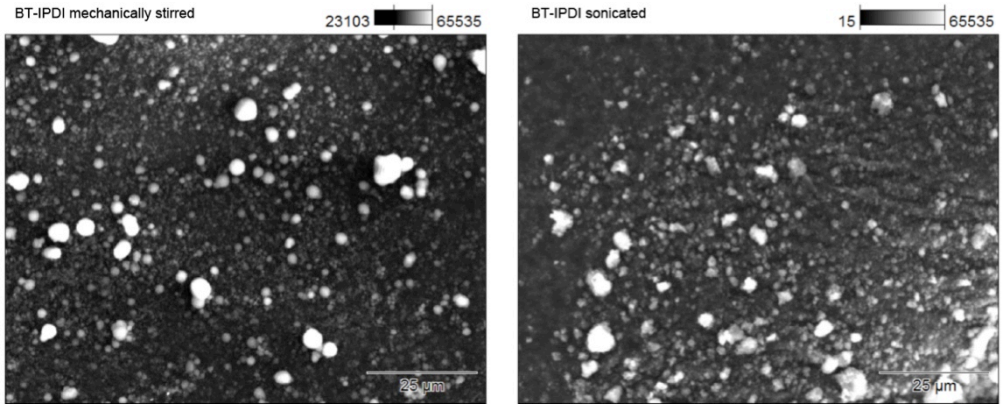

Figure 40: SEM images of BT-IPDI mechanically stirred (15 keV; 1000x; left) and BT-IPDI sonicated (15 keV; 1000x; right).

When comparing the different types of BT-IPDI in Figure 40, a first observation is that the mechanically stirred capsules (1 – 5 µm) are relatively smaller than the mechanically stirred GT-IPDI capsules (7 – 25 µm). This is probably due to the fact that the viscosity of the BT prepolymer mixture is much less than the viscosity of the GT prepolymer. Therefore, much less energy is needed to agitate the mixtures and when applying the same energy (in this case either by stirring at the same RPM or by sonication with the same input values) much smaller oil droplets can be formed in the emulsion resulting in overall smaller microcapsules. A second observation is again that the synthesized microcapsules by means of sonication (≤ 1 µm) are smaller than the ones produced by mechanically stirring (1 – 5 µm). However, the difference is size is much less pronounced than for the GT microcapsules.

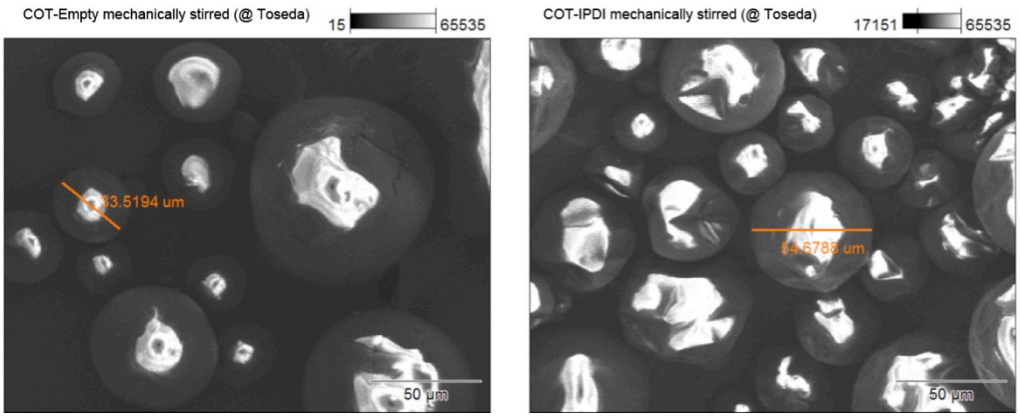

Figure 41: SEM images of COT-Empty mechanically stirred (5 keV; 500x; left) and COT-IPDI mechanically stirred (5 keV; 500x; right).

When looking at the SEM images of COT-Empty and COT-IPDI microcapsules, it can be observed that the capsules lost their spherical form. As said before, the T_g of the COT microcapsules is 17 °C which means they are ductile at room temperature. Therefore it could be that the PU shell deforms due to the low pressure in the vacuum chamber of the SEM. The size of both types of capsules ranges between 10 – 70 µm. This is in line with the previous observations that capsules that are synthesized by mechanical stirring are larger than the sonicated capsules.

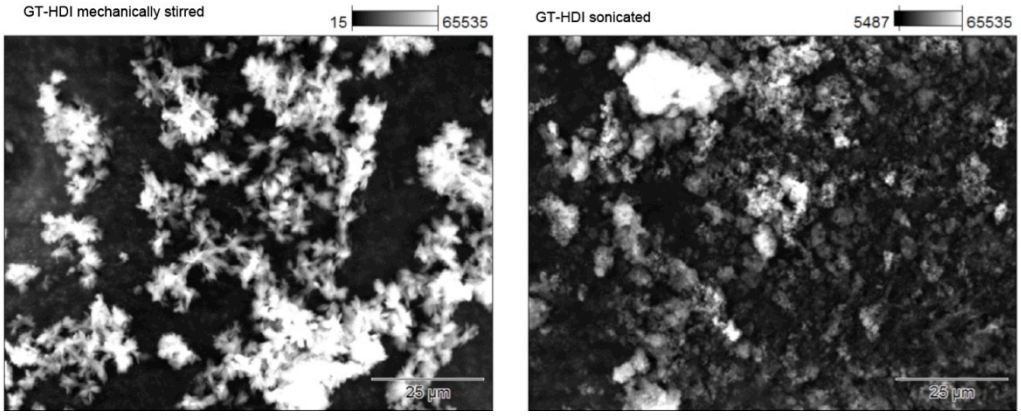

Figure 42: SEM images of GT-IPDI mechanically stirred (15 keV; 1000x, left) and GT-HDI sonicated (5 keV; 1000x; right).

When looking at the micrographs of both types of GT-HDI, it is clearly seen that no capsules were formed. Probably HDI was too reactive and the polyol chain extender reacted with both the added healing agent HDI and the TDI based prepolymer forming powder instead of capsules. A possible solution for this problem is to synthesize the prepolymer with the aromatic diisocyanate methylene diphenyl diisocyanate (MDI) for the encapsulation of HDI instead of toluene diisocyanate (TDI). This was already proposed by Huang et al. [42].

1.8. Thermal analysis

It was tried to determine the amount of liquid content of the GT microcapsules. This was done by performing TGA analysis of GT-Empty and two types of GT-IPDI. These two types of GT-IPDI were both produced by sonication, however the used prepolymers had a slightly different solid content (respectively 30 wt% and 25 wt%) resulting is a slightly altered viscosity of the prepolymer/cyclohexanone mixture.

A lot of degradation steps of the microcapsules are seen at different temperatures from the TGA measurement. The interpretation of the TGA measurement (Figure 43 and 44) is not so straightforward. When comparing the GT-IPDI and the GT-IPDI 2 microcapsules, one possibility is that microcapsules with a different size distribution are formed, due to the difference in used prepolymers. And therefore it is also possible that they have a different mechanical strength distribution. Consequently, some capsules are stronger than others. It is also assumed that there is pressure build-up before the microcapsules burst open, making it more difficult to determine which peak resembles which degradation.
The assumed liquid core of the microcapsules is a mixture of IPDI and cyclohexanone for the GT-IPDI type and pure cyclohexanone for the GT-Empty type. To get a better understanding of the liquid core and to identify the different peaks, an experiment with a TGA mass spectrometer should be performed. Also the crushed microcapsules, after washing with a solvent to remove the liquid core, should be investigated in order to determine the peak that resembles the degradation of the PU shell wall.

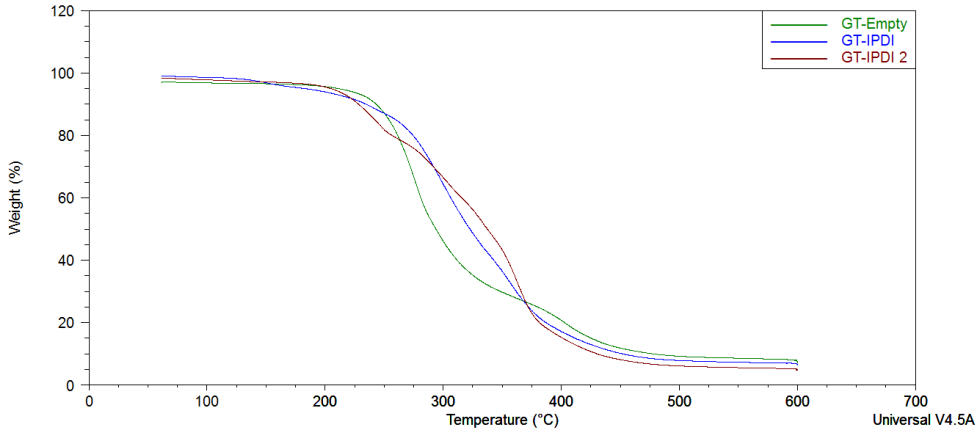

Figure 43: TGA measurement of GT-Empty (green), GT-IPDI (blue) and GT-IPDI 2 (red). Heating rate: 20 °C/min; Purge gas: N_2. Weight (%) as a function of temperature (°C).

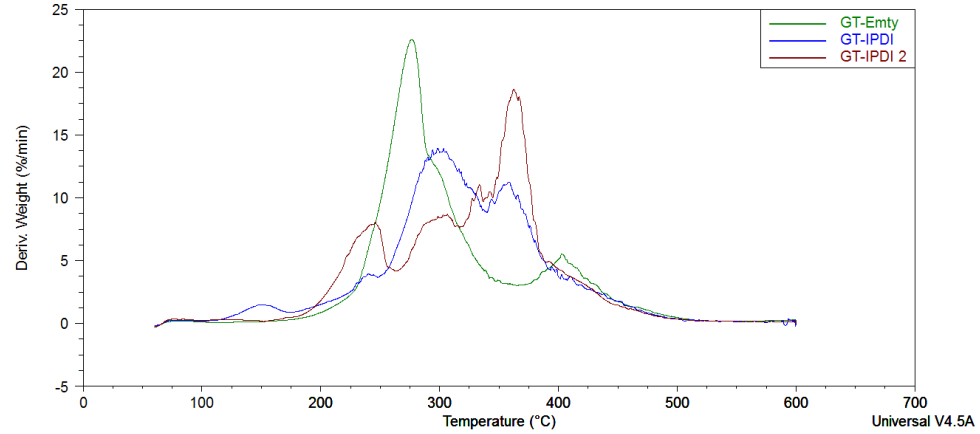

Figure 44: TGA measurement of GT-Empty (green), GT-IPDI (blue) and GT-IPDI 2 (red). Heating rate: 20 °C/min; Purge gas: N_2. Deriv. weight (%/min) as a function of temperature (°C).

A second attempt on trying to determine the amount of liquid content of the capsules was made by using DSC to find back the characteristic crystallization peaks of the components cyclohexanone and IPDI that make up the liquid content. Therefore these pure components were analysed first separately, and then their mixture, before analysing the capsules.

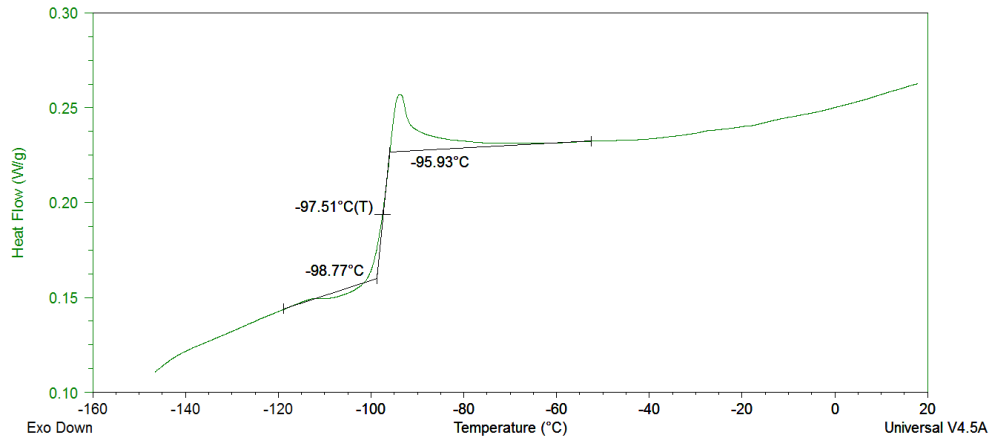

Figure 45: DSC measurement of pure IPDI from -150 °C to 20 °C showing T_g at -97,5 °C. Heating rate: 10 °C/min.

From Figure 45 it was seen that the glass transition temperature of IPDI is -97,5 °C at a heating rate of 10 °C/min. No crystallization peak was observed although it was expected to see a crystallization peak.

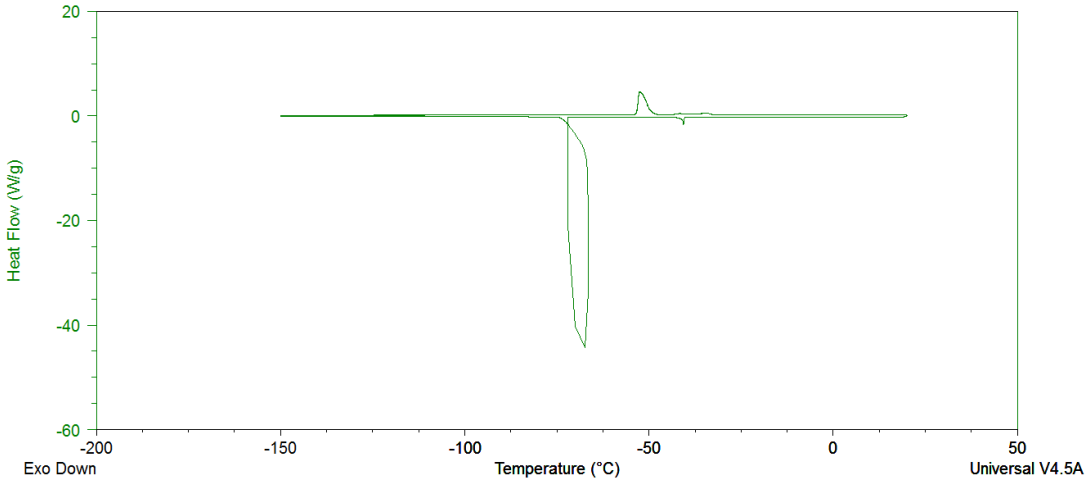

Figure 46: DSC measurement of pure cyclohexanone from -150 °C to 20 °C. Heating rate: 10 °C/min.

From the DSC measurement of pure cyclohexanone, two peaks are observed. An enormous crystallization peak (-65 °C) that shows a loop because of the exothermicity of the crystallization process; heat is released faster than that the DSC can cool, thus creating this effect. The second peak (- 50 °C) is an endothermic peak resembling the melting of pure cyclohexanone.

The liquid core of the microcapsules is a mixture of cyclohexanone and IPDI. Therefore, it was tried to analyse a mixture of both components with a ratio that resembles the assumed ratio inside the capsules. Unfortunately the measurements of this mixture were not successful in determining characteristic peaks (data not shown). Probably the first problem of analysing this mixture was the opening of the DSC crucible because they were put into an oven that still had an increased temperature. Then to avoid this problem of crucible opening, the crucible was inserted in the DSC at a temperature of -20 °C. Probably because of ice formation around the DSC sensor, due to the opening at such a low temperature, the measurement was disturbed again and no good signal was measured. In future work this experiment has to be redone by opening the DSC oven at a temperature just above 0 °C. This has to be combined with the analysis of microcapsules at a temperature range between -150 °C (or even a bit lower) and 200 °C to try to find back characteristic peaks of the prepolymer/ cyclohexanone mixture as this experiment was not performed.

As seen in the TGA results in Figure 44, the degradation of the microcapsules starts at a temperature higher than 200 °C. Therefore, the microcapsules were analysed with DSC till 200 °C, which is shown in Figure 47. A glass transition temperature is observed at 105 °C (at a heating rate of 10 °C/min) which is in good agreement with the glass transition temperature measured by Toseda. An important remark is that the heating rate of the experiments done by Toseda is 20 °C/min whereas here the glass transition temperature is determined at a heating rate of 10 °C/min and therefore the obtained glass transition temperatures may not be compared.

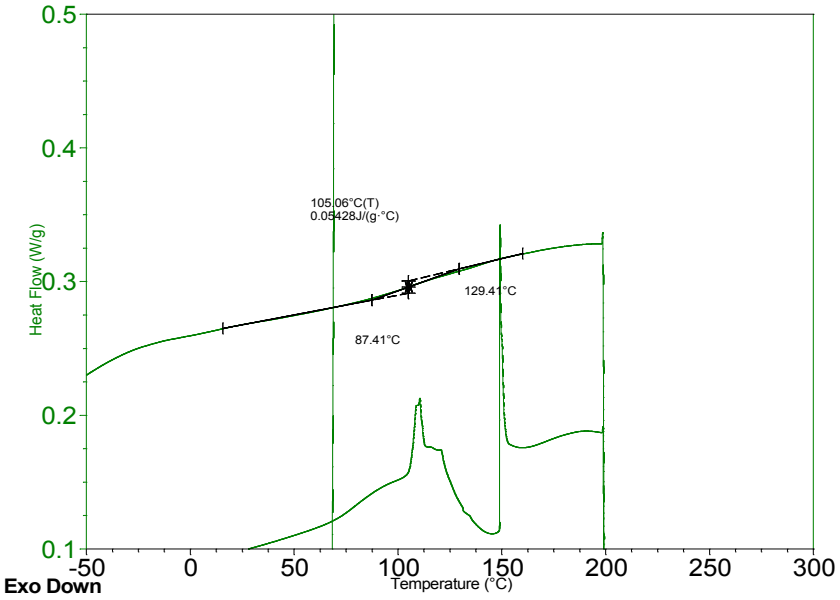

Figure 47: DSC measurement of GT-IPDI microcapsules showing a T_g at 105 °C. Heating rate: 10 °C/min.

1.9. Conclusions of the microcapsule synthesis

The synthesized types of prepolymer were all TDI based prepolymers with three different polyols (glycerol, 1,4-butanediol and castor oil). All prepolymer mixtures showed NCO terminal end groups that were able to react further during the interfacial polymerization in order to form microcapsules. Based on the obtained results it can be concluded that all synthesized types of prepolymer were successful.

By comparing the FTIR results from microcapsules without addition of the healing agent IPDI and the prepolymer, it was observed that the prepolymer fully reacted to form a PU linkage. From the FTIR results of microcapsules with and without addition of the healing agent IPDI it was seen that IPDI was encapsulated for the three different types of microcapsules (GT, BT and COT). However the determination of the amount of liquid content in the core of the microcapsules by means of thermal analysis did not succeed.

A relation between the agitation method and the microcapsule size was confirmed through SEM analysis. Further it is noticed that the microcapsules produced with the BT prepolymer mixture and 1,4-butandediol as chain extender were overall smaller than the GT microcapsules. The reason for this is probably the viscosity of the BT prepolymer mixture, which was much lower than for the GT prepolymer mixture. Less energy was thus needed to create smaller oil droplets. It was also shown that the COT microcapsules showed a wrinkled and deformed surface, which is probably because of the low glass transition temperature, causing the capsules to be ductile at room temperature.

The usage of HDI as a healing agent was confirmed to be a very interesting path to follow as the reactivity was much higher than for IPDI with water from the environment as was shown by means of a TAM measurement. Unfortunately, the formation of GT-HDI capsules was unsuccessful. However, for future work it should be attempted to produce an MDI based prepolymer and to use this for the synthesis of microcapsules containing HDI as a healing agent.

The next step in this work is the incorporation of the synthesized GT microcapsules in a PU coating and to test their self-healing ability.

2. Synthesis and analysis of self-healing coatings

2.1. Introduction

Polyurethanes (PU) are produced by a condensation reaction of isocyanate-bearing species (NCO) and molecules with hydroxyl functionality (OH). Polyurethanes can either have a chemical structure of a thermoplastic or a thermoset and can have a physical structure of a solid, an elastomer or foam. Various combinations are thus possible depending on the specific isocyanate bearing species and polyol that are used. In this work, the polyurethane is formed by the condensation reaction between a diisocyanate and a polyol, more specifically a triol resulting in a hard thermoset. A PU thermoset is very suited to use as a coating and has good corrosion protection of the underlying substrate. In order to get coatings that are able to self-heal, the synthesized GT microcapsules containing the healing agent IPDI were dispersed in such a PU coating. The mixture containing the dispersed microcapsules was applied on a steel substrate with a wire wound coater. The synthesized PU coatings contained different weight percentages of GT-IPDI microcapsules. After coating synthesis, Electrochemical Impedance Spectroscopy (EIS) and Atomic Force Microscopy (AFM) were performed to test the coatings on their self-healing ability, by performing measurements before and after the application of a defect and after immersing the damaged coatings in water for several days.

2.2. Synthesis of self-healing coatings

The coating formulation was based on the synthesized GT prepolymer. Mainly two types of prepolymer/cyclohexanone mixtures were used to prepare the coating. A prepolymer content of approximately 30 wt% was used for the coating formulation. However some coatings were prepared with a prepolymer mixture containing 50 wt% of prepolymer, which was more viscous than the other prepolymer mixture. It was observed that in the coatings that were produced with the second type of prepolymer mixture, a lot of bubbles were created. This is probably due to the high viscosity; the bubbles cannot leave the coating and are trapped. For the further analysis, only the coatings without bubbles were selected.

Different amounts of microcapsules were added at room temperature in order to create formulations with a concentration of 0, 5, 10, 15 and 20 wt% of GT microcapsules incorporated in the coatings. The dispersion was performed by placing the formulation in a sonic bath for 10 to 30 minutes. An important remark is that some of the microcapsules stuck to the bottom of the beaker when they were dispersed in the coating. The amount of glycerol, to allow the prepolymer to react completely, was calculated and added dropwise. The mixture was applied on a Q-panel steel substrate with a wire wound bar coater with a theoretical wet thickness of 100 and 500 µm The coatings were left for 24 hours to cure and to let the solvent cyclohexanone evaporate.

A complete list of synthesized PU coatings with their microcapsule content and the used prepolymer can be found in the Appendix.

2.3. FE SEM images of the synthesized coatings

Several coatings were investigated by means of FE SEM after depositing a nanolayer of platinum/palladium on top of the PU coating to make the surface conductive. This technique was performed in order to check the coating morphology and to try and identify the dispersed microcapsules at the surface of the PU coating.

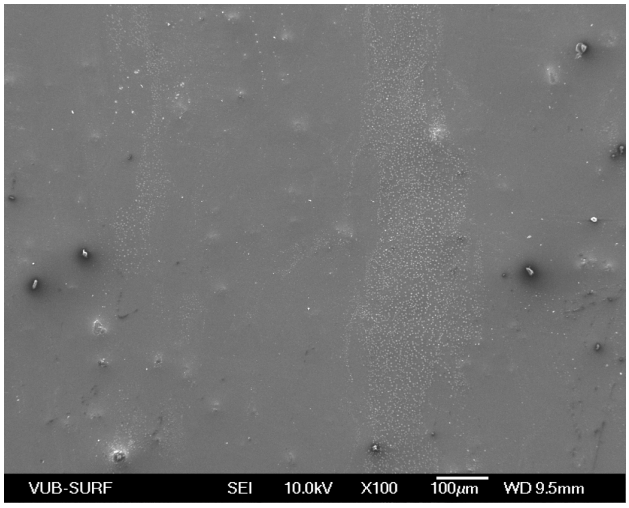

Figure 48: FE SEM image of Coating_5wt% (Coating 14 in Appendix); Wet thickness: 100 µm; Average dry thickness: 23 µm.

Figure 48 shows a PU coating containing 5 wt% of sonicated GT microcapsules at a magnification of 100x. It is assumed that the small white dots that are visible are the dispersed microcapsules. From Figure 48 it can also be seen that the microcapsules form regions where the concentration of the microcapsules is denser than other regions. This is an indication that the dispersion of the microcapsules in the coating formulation has to be improved in order to get a more uniform distribution. In Figure 49, a magnification of the white dots is shown. The charge build-up as well as the size (average 1 µm) of the spheres suggests that these are the microcapsules.

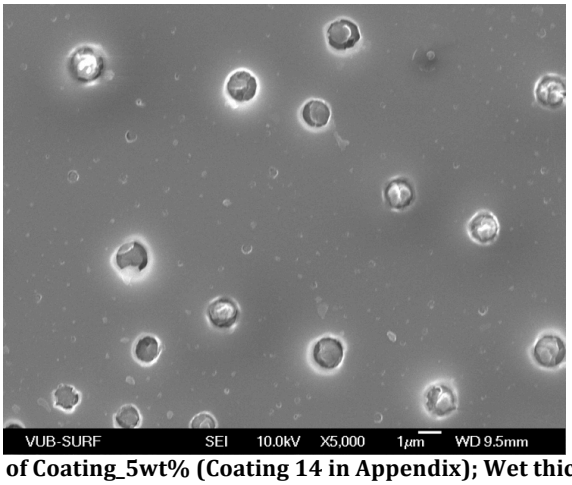

Figure 49: FE SEM image of Coating_5wt% (Coating 14 in Appendix); Wet thickness: 100 µm; Average dry thickness: 23 µm.

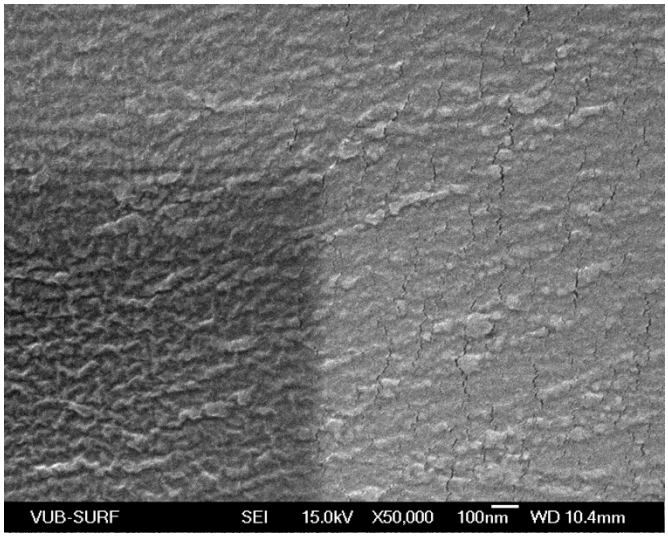

Figure 50: FE SEM image of Coating_10wt% (Coating 5 in Appendix); Wet thickness: 100 µm; Average dry thickness: 28 µm.

Caution is advised when analysing the morphology of the coatings. Notwithstanding that the coatings were covered with a conductive metal layer, charge build-up was still possible. This charge build-up altered and even damaged the coating surface as can be seen in Figure 50. The dark area is due to the electron beam of the FE SEM and probably the vacuum created the cracks in the less dark region. Therefore, it is also not advised to investigate self-applied scratches in the coating and whether they are healing. The change that might be attributed to healing could be due to electron beam damage.

2.4. EIS measurements of the synthesized coatings

Electrochemical Impedance Spectroscopy measurements were performed to test the properties of the synthesized self-healing coatings with different concentrations of sonicated GT microcapsules. Coatings with 0, 5, 10 and 20 wt% of microcapsules were tested: undamaged, just after the application of a scratch and after certain times of immersion of the scratched sample in water. The immersion in water is done to accelerate the possible healing action. Also blank steel substrates, with and without titanium conversion pre-treatment, were tested as reference. Additionally several samples of the same coating were tested to compare if the properties of the coating were uniform.

Table 1: Overview of the PU coatings used in EIS experiments.

EIS	Name in Appendix	Wet thickness (µm)	Avg. dry thickness (µm)	Ti conversion
NoCoating_NoTi	/	0	0	No
NoCoating_Ti	/	0	0	Yes
Coating_0wt%	Coating 9	100	17	No
Coating_5wt%	Coating 1	100	18	No
Coating_10wt%	Coating 5	100	28	No
Coating_20wt%	Coating 23	100	38	Yes

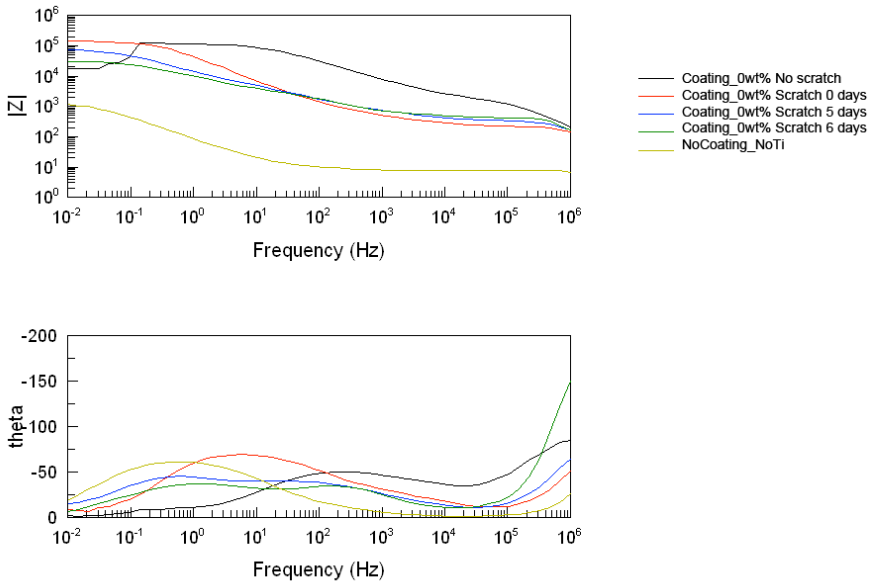

Figure 51: Bode plots of Coating_0wt% before and after application of a defect and after immersion in water for 5 and 6 days.

In Figure 51, the Bode plots of the coating without microcapsules are shown. The impedance modulus of the coating is higher than the substrate without coating, meaning that the coating has some barrier function. However, the impedance values are rather low and this indicates that the coatings are of poor quality regarding their protective properties. It is assumed that an artefact is seen at low frequencies (10^{-2} – 10^{-1} Hz) for the unscratched coating and it is assumed that the impedance modulus should be higher than after the application of the defect. Given the previous assumption, the results can be logically explained. As there are no microcapsules embedded in the coating, the pore resistance drops after the application of the scratch and it drops even further after 6 days of immersion in water. This is because the coating lost some of its protective barrier function and water and electrolyte can enter through the applied defect, as well as penetrate the pores of the coating towards the substrate.

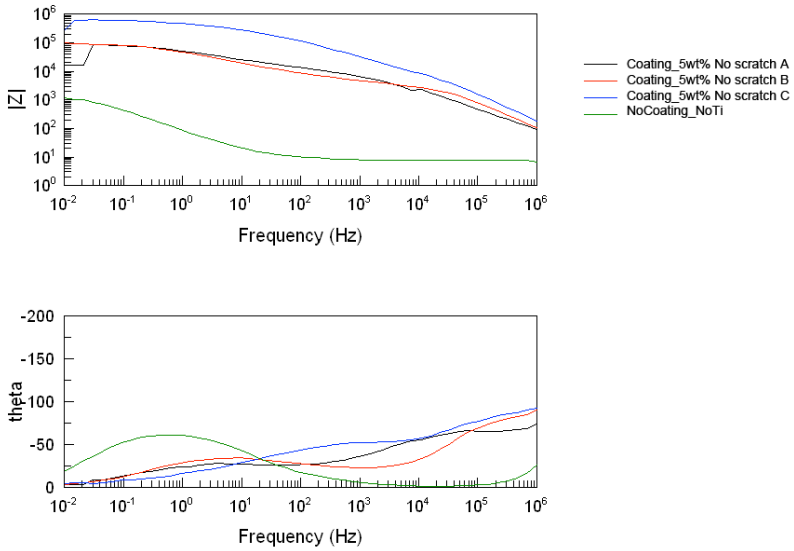

Figure 52: Bode plots of Coating_5wt% without application of a defect, measurements performed at three different areas of the same coating.

When looking at the Bode plots of three different areas of the same coating (Figure 52) in order to see whether the coating properties are uniform, it is seen that this is not the case. The pore resistance is different at three different places. This means the coating properties are not uniform, which means that the way of applying the coating formulation has to be altered. As the coating formulation is applied manually on the steel substrate, the used speed and pressure deviates tremendously. This results in highly non-uniform coatings.

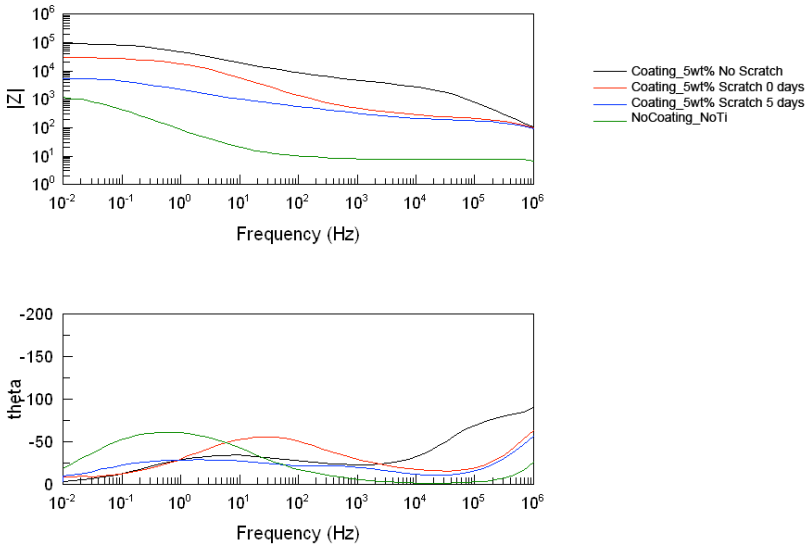

Figure 53: Bode plots of Coating_5wt% before and after the application of a defect (made by sharp tip tool) and after immersion in water for 5 days.

The Bode plots of a coating with 5 wt% are shown in Figure 53. Unfortunately, no healing effect is observed after the application of a defect by means of a sharp tip. This coating also has poor barrier properties, which is seen from its low impedance modulus in comparison with the uncoated steel substrate. The impedance modulus keeps dropping after immersion in water of the scratched substrate, which indicates that no healing has taken place.

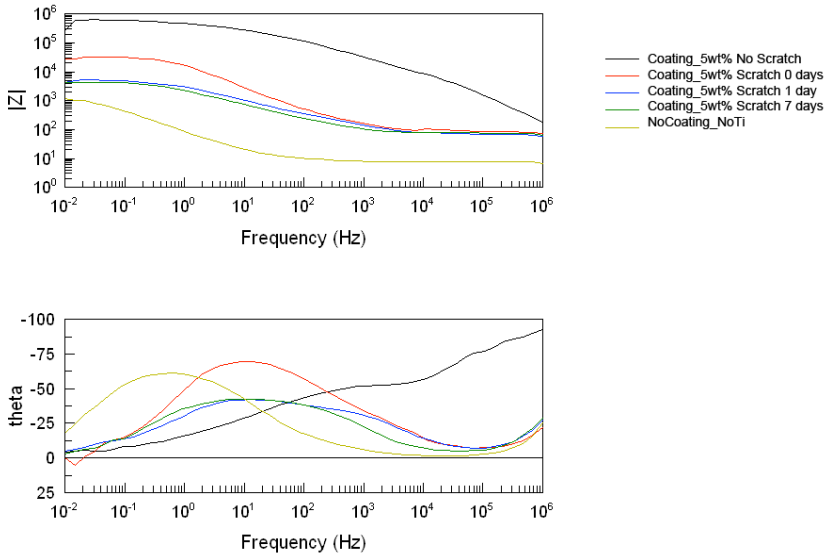

Figure 54: Bode plots of Coating_5wt% before and after the application of a defect (with a scalpel) and after immersion in water for 7 days.

In Figure 54, the Bode plots of the coating with 5 wt% is shown with and without a scratch and after immersion in water. The difference with the previous Bode plots from Figure 53 is that the applied defect was this time a scratch made with a scalpel. The scratch was about 0,5 cm wide. The same conclusions can be made as previous Bode plots. Unfortunately, no indication of healing was observed.

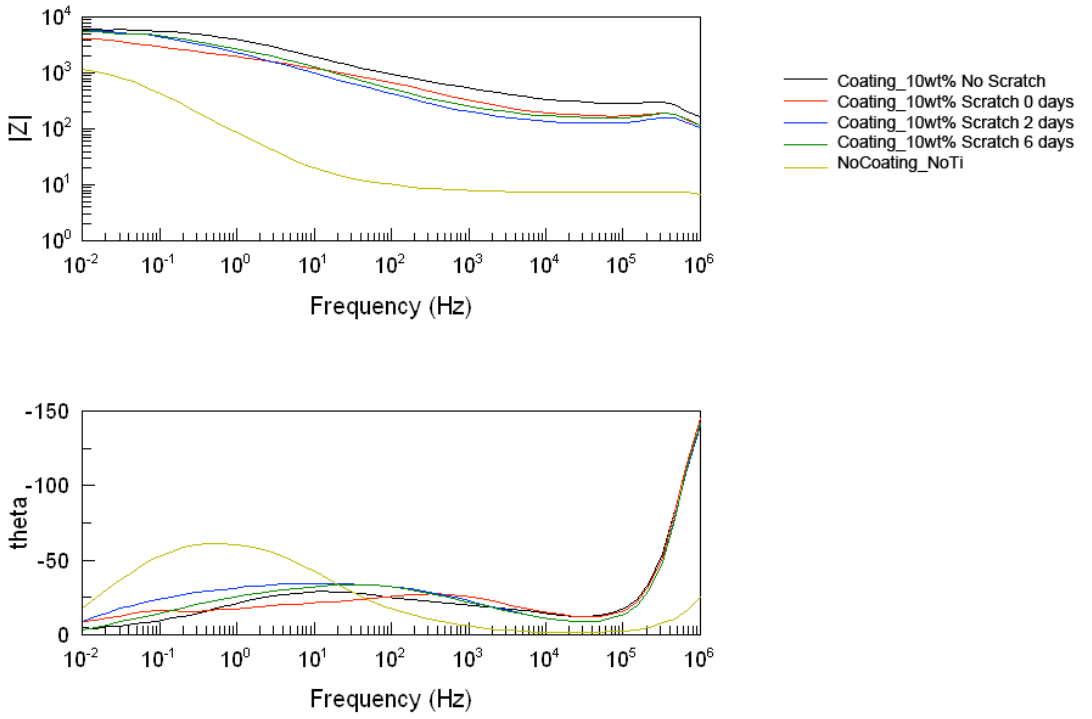

Figure 55: Bode plots of Coating_10wt% before and after the application of a defect and after immersion in water for 6 days.

When looking at the Bode plots of Coating_10wt%, it is seen that after the application of a defect with a sharp tip, the impedance modulus drops (red line). However, after the immersion in water, the impedance modulus in the lowest frequency range starts to increase and goes up to the initial impedance modulus of the undamaged sample (blue and green line). In the medium frequency range, the impedance modulus is still a bit lower than the undamaged substrate after 2 days of immersion indicating that the barrier properties are decreasing. It is possible that this (small) decrease in barrier properties is due to the degradation of the coating in time when immersed in water. The degradation over time of the coating properties when immersed in water has to be investigated in the future. But when comparing the impedance modulus of Coating_10wt% after 2 days of immersion (blue line) and after 6 days (green line) in the medium frequency range, it is observed that the modulus has increased. The green line is higher than the blue one, which indicates a recovery of barrier properties. Together with the increase in impedance modulus in the lowest frequency range, this is an indication that something has happened and that healing might have taken place.

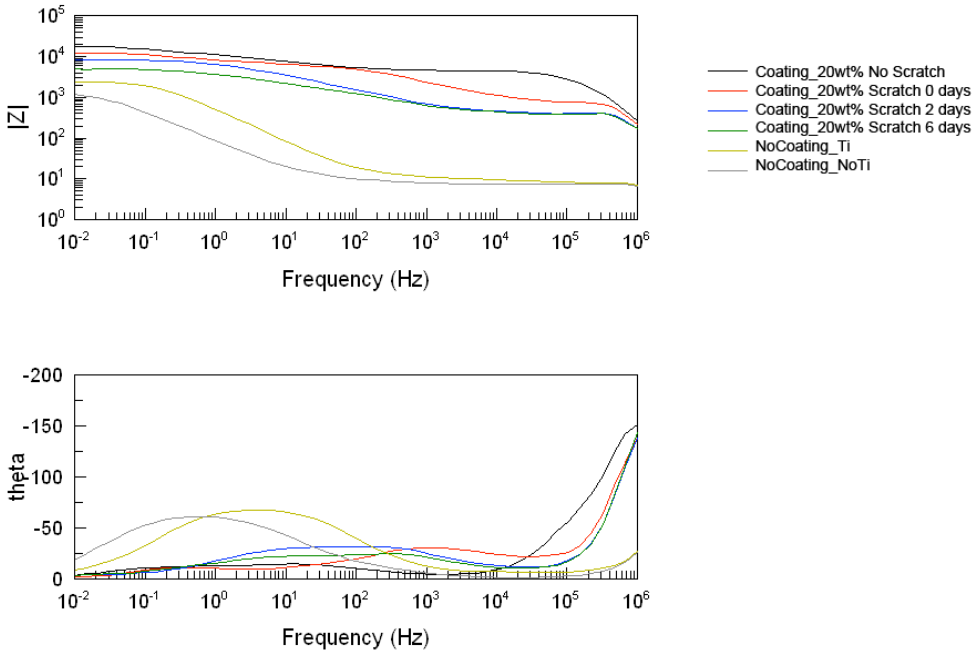

Figure 56: Bode plots of Coating_20wt% before and after the application of a defect and after immersion in water.

Looking at Figure 56, which shows the Bode plots of Coating_20wt%, the impedance modulus drops a little for the complete frequency range after the application of a defect. When immersed in water for 6 days, this decrease continuous. Unfortunately, no indication of healing is observed.

After observing the coatings with 0, 5, 10 and 20 wt% of sonicated GT microcapsules, only for the coating having a concentration of 10 wt% of microcapsules some indication of healing is observed. Another observation was that the overall quality of the coatings was rather poor. Therefore in the future, these experiments have to be redone in order to check the reproducibility of the result. Moreover optimizations of the dispersion of the microcapsules in the coating formulation, an optimization of the coating formulation and an improved way of application have to lead to an improved self-healing coating system.

2.5. OM images of the synthesized coatings

In order to see whether something has changed, the samples used in the EIS analyses of Coating_0wt% (Figure 57) and Coating_10wt% (Figure 58) were compared after 6 days of immersion in water by means of an optical microscope.

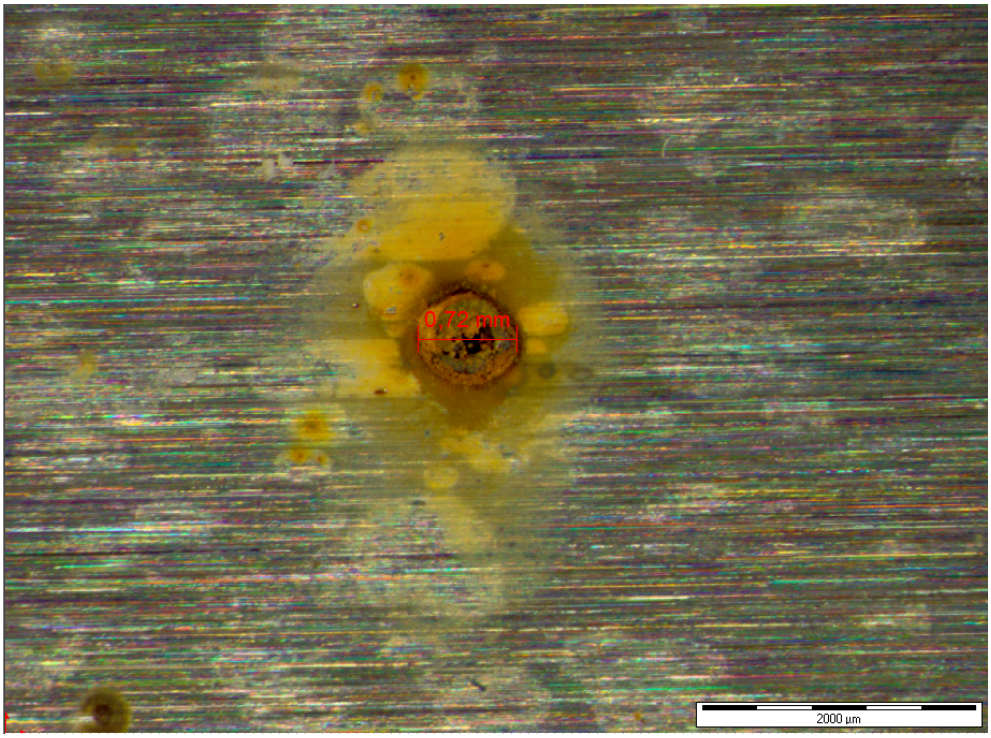

Figure 57: OM image of Coating_0wt% after 6 days of immersion in water. 100x magnified.

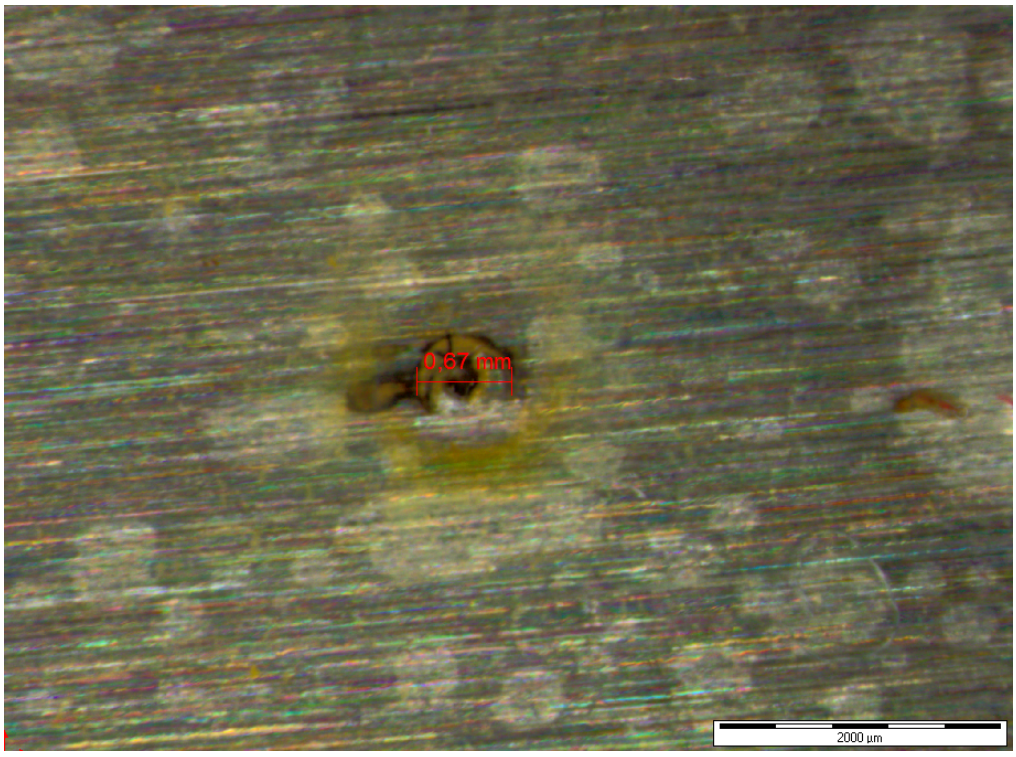

Figure 58: OM image of Coating_10wt% after 6 days of immersion in water. 100x magnified.

When looking at both OM images, it is clearly seen that something is different. The corrosion of the substrate at the defect is strong for the coating without microcapsules whereas for the coating containing 10 wt% of sonicated GT microcapsules, the corrosion is much less pronounced. This is in accordance with what was observed in the EIS measurements.

2.6. AFM images of the synthesized coatings

Another technique that was used to investigate the coatings was AFM. More specifically, this technique was used to investigate whether healing could take place at a local defect.

Coatings containing a concentration of 0, 5, 10, 15 and 20 wt% microcapsules were analysed after the application of a scratch of approximately 0,5 cm with a scalpel. Images of the applied scratch are made before and after immersion in water for a certain time. In table 2, an overview of all the coatings that were analysed with AFM is shown.

All these coatings were analysed by means of AFM, however only for Coating_15wt% the images before and after immersion in water can be compared. Therefore, only these results are presented.
It was very hard to find back the exact same spot of the scratch with the AFM after the samples were immersed in water. It is however thought that for Coating_15wt%, approximately the same spot is retrieved each time. In the future the localisation of the exact same spot should be facilitated for example by the use of nano-indentation to mark an area. The indentations could be found back with the AFM and then they could be used as reference points. However, the risk exists that these reference points might disappear due to healing of the coating.

The coatings were measured with a coating thickness gauge at 10 measure points. Due to the high non-uniform coatings and the error on the gauge, the deviation of the average thickness is approximately 5 µm.

Table 2: Overview of the PU coatings used for AFM measurements

AFM	Name in appendix	Wet thickness (µm)	Avg. dry thickness (µm)	Ti conversion
Coating_0wt%	Coating 9	100	17	No
Coating_5wt%	Coating 1	100	18	No
Coating_10wt%	Coating 6	100	33	No
Coating_15wt%	Coating 21	100	26	Yes
Coating_20wt%	Coating 23	100	38	Yes

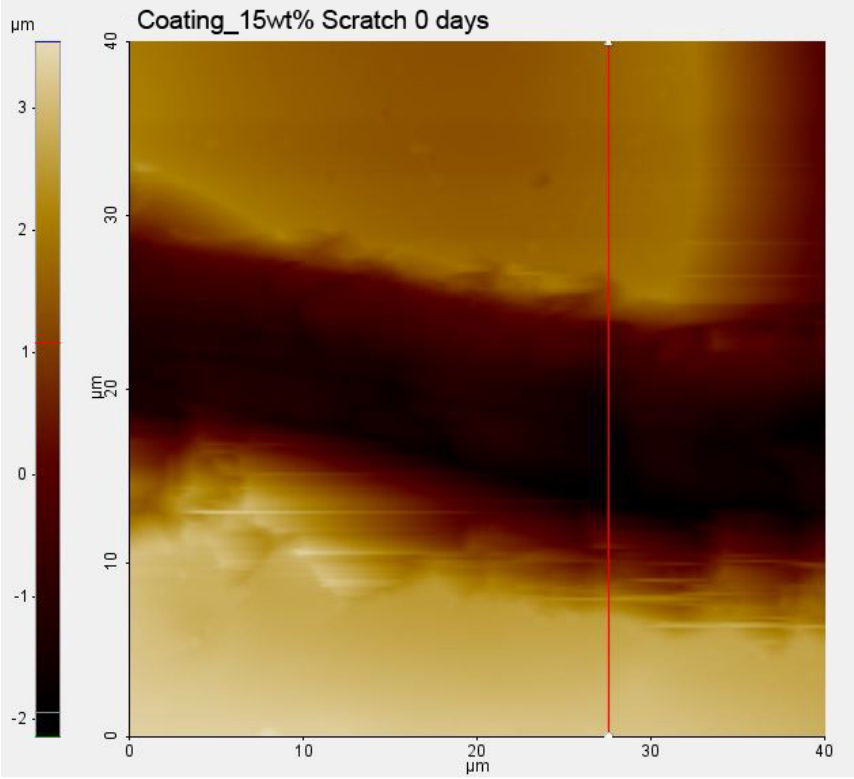

Figure 59: AFM image of a scratch applied on Coating_15wt% just after application.

When looking at Figure 59, the scratch is clearly observed. This AFM measurement shows the scratch just after its application. The width of the scratch is approximately 10 - 15 µm.

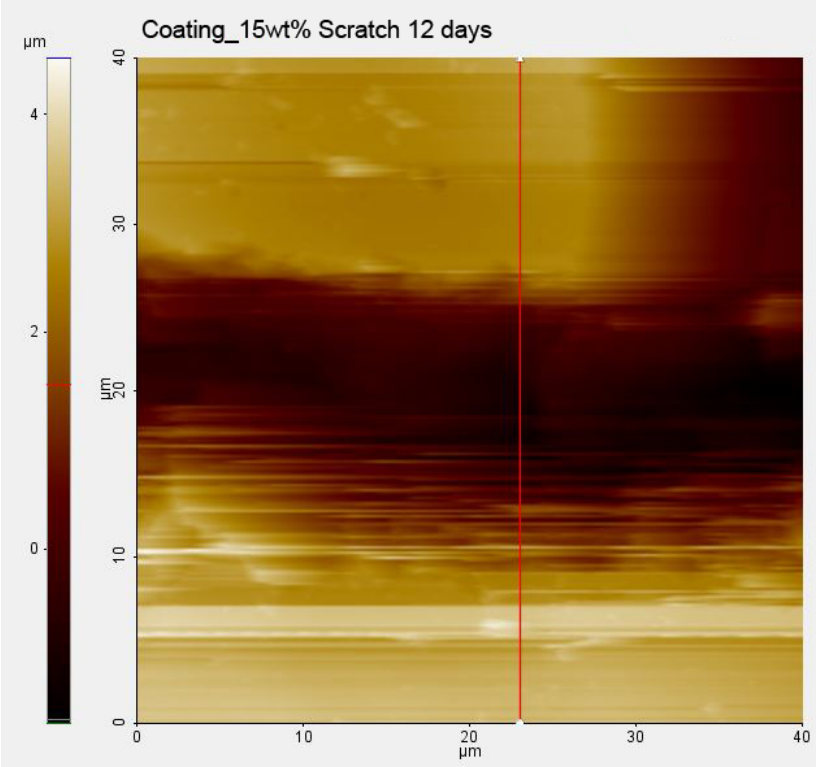

Figure 60: AFM image of a scratch applied on Coating_15wt% 12 days of immersion in water.

In Figure 60, an AFM measurement of the scratch is shown after 12 days of immersion in water. At first glance, some change is observed. The red line on both Figures 59 and 60 resembles the place of the line scan, which is shown in Figure 61 for the coating just after application of the scratch and in Figure 62 for the coating after immersion in water for 12 days.

Figure 61: Line scan of red line shown in Figure 59 (Coating_15wt% 0 days).

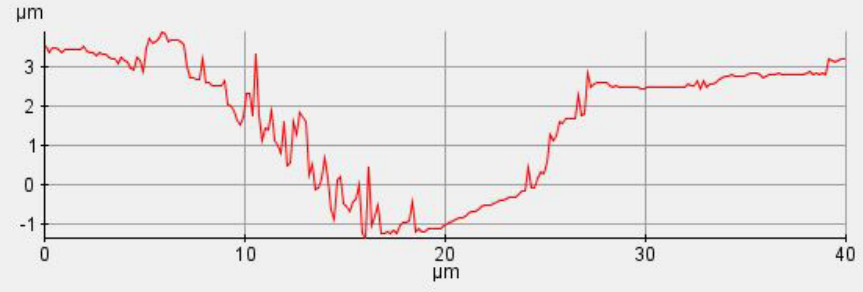

Figure 62: Line scan of red line shown in Figure 60. (Coating_15wt% 12 days)

When looking at both line scans, it can be seen that some difference is observed. It seems that the depth of the scratch dropped from approximately 5 µm to approximately 4 µm. This could be an indication of healing. However, when looking to the right side of the scratch, where no noise is observed, no change is observed therefore, it is concluded that no indication of healing is observed.

A strong fluctuating profile is observed between 5 – 20 µm in Figure 62. This is probably due to some organic material sticking to the tip while the tip was scanning.

As mentioned, caution should be taken when considering this data. The possibility exists that two different places are being compared with each other and that there is no healing. In future experiments, retrieving and comparing the exact same location should be a major focus. Next to this point, the reproducibility of this result should be checked, as it was not possible to reproduce these observations.

2.7. Conclusions of the coating synthesis

PU coatings with different concentrations of dispersed sonicated GT microcapsules were synthesized. The organic coatings were analysed by means of FE SEM, however this technique is not very suited to analyse manually applied defects as the primary electron beam itself could alter and create defects in the coating. The microcapsules could be observed, but it was also seen that the dispersion of the microcapsules is not uniform and that there exist dense and

less dense regions of them. Together with the observation that during the synthesis of the coating formulation some microcapsules stuck to the bottom of the beaker, it can be said that the method of dispersing the microcapsules has to be improved.
The quality of the coatings was evaluated by means of EIS and from these measurements it was seen that the overall quality of the coatings was rather low. This was probably due to the way of application and the quality of the coating formulation as it might be that the used ratios of diisocyanate and polyol are not correct. To improve the quality of the coatings one suggestion is the use of an automatic wire wound applicator so that the coating is more uniform. Another idea is the use of commercial prepolymer or PU coating formulations as here the ratios of polyol and diisocyanate are correct and additives are added. The self-healing property of the coatings was analysed by means of EIS and AFM. From EIS measurements, after the strong decrease of the barrier protection when the scratch was applied, a clear increase of the coating barrier protection was observed after the scratch was let to heal by immersion in water. This is an indication that the concept works. However, this result was only observed for one of the synthesized coatings. Therefore, the experiments have to be redone in order to reproduce the obtained results. No indication of healing was observed by AFM. A difficulty that exists is to retrieve the exact same spot of the analysed coating. The use of nano-indentation to mark reference points is a possible solution for this problem, however the risk exists that these points disappear due to the healing.
For the evaluation of the self-healing ability by both EIS and AFM, a problem is the scratch application. This was now done with a sharp tip and a scalpel respectively, but these scratches are not exactly repeatable. In the future a way has to be found to apply uniform scratches in order to be able to better repeat the experiments and compare the obtained results. It is possible to create small micro-defects by means of nano-indentation in order to analyse the possible healing of micro-defects.

V. Conclusions

1. General conclusions of this work

Several types of prepolymer were successfully synthesized. These prepolymers were all TDI based. Three different types of polyol were used to synthesize three types of prepolymer, these polyols were the triol glycerol, the diol 1,4-butanediol and the triol castor oil. Thanks to FTIR analysis it was observed that the prepolymers had PU linkage and together with the relative viscous mixture it could be concluded that a intermediate molecular weight product was synthesized. All these synthesized prepolymers had NCO terminal end groups and thus they could be used in an interfacial polymerization reaction to produce the capsule shell wall.
After the production of microcapsules, a comparison of the FTIR spectra of the different types of produced microcapsules containing the healing agent IPDI and the microcapsules where no healing agent was added to the oil phase, along with the spectrum of the prepolymer, showed an interesting result. It could be concluded that the healing agent IPDI was successfully encapsulated. When comparing the spectra of the prepolymer with the empty capsules it was seen that the NCO terminal groups of the TDI based prepolymer were completely reacted to form the microcapsule shell wall. By means of SEM analysis, a direct relation between the agitation speed and the size of the microcapsules was confirmed. It was seen that the viscosity of the prepolymer/cyclohexanone mixture plays an important role in the size of the microcapsules. When the same agitation method was used, the BT microcapsules were smaller than the GT microcapsules. This is probably due to the lower viscosity of the BT prepolymer mixture and therefore smaller oil droplets were made in the emulsion during the interfacial polymerization. Further it was also observed that spherical capsules were synthesized for the three different types of microcapsules (GT, BT and COT), however the COT microcapsules showed a deformed spherical shape, which was not the case for the other types of microcapsules. This is probably due to the low glass transition temperature of the COT microcapsules and therefore the shell wall having a relative low mechanical strength, which leads to a deformation by the electron beam and the low pressure in the vacuum chamber. Next to the use of IPDI as a healing agent, the aliphatic diisocyanate HDI was confirmed to be an interesting healing agent by means of a TAM measurement. This TAM measurement mimicked the relative humidity conditions in Brussels and it was shown that HDI reacts much faster with water from the environment than IPDI does. Therefore, HDI is more suited to encapsulate as a healing agent as it will result in faster healing reactions. In this work it was tried to encapsulate the healing agent by using a glycerol TDI based prepolymer and glycerol as chain extender, but unfortunately this did not succeed. The determination of the amount of liquid content by means of thermal analysis was also not successful.

Coatings with different concentrations of sonicated GT microcapsules were synthesized. It was seen by means of FE SEM that the dispersed microcapsules formed dense and less dense regions. Due to charge build-up FE SEM is not suited to investigate the coatings as they induce damages even though a small

conductive layer was sputtered on top of the coatings. The quality and the self-healing ability of the coatings were analysed by means of EIS and AFM. It was seen that the overall quality of the coatings was poor. For the self-healing ability of the coatings, only for one coating an indication of healing of the scratch applied with a sharp tip was observed by EIS. This coating containing 10 wt% of GT microcapsules was optically compared with a coating containing 0 wt% after immersion in water for 6 days. A clear difference in amount of corrosion was observed. By looking inside the scratch applied with a scalpel of a coating containing 15 wt% of GT microcapsules by means of AFM, no indication of healing was observed at the bottom of the scratch. However, it is not completely sure whether the observation of the AFM was done at the exact same spot.

This work provides a lot of qualitative results on the synthesis of microcapsules that encapsulate the healing agent IPDI and shows promising indications on the self-healing property of the synthesized coatings. However, several parameters still have to be optimized in order to get high quality and autonomous self-healing coatings. Additionally, this work provides a lot of interesting suggestions and ideas that can be explored further.

2. Future prospects

The encapsulation of the aliphatic diisocyanate healing agent HDI was unsuccessful. A possible solution to the encapsulation of HDI is to produce the microcapsules with a MDI based prepolymer. An alternative to the encapsulation of the diisocyanate HDI, that reacts faster than IPDI, is to use microcapsules containing IPDI in combination with a corrosion inhibitor that is incorporated into the coating or even is encapsulated inside the microcapsule. The corrosion reaction will then be inhibited while the healing agent has time to react with the water from the environment in order to heal the coating.

A way should be found to determine the amount of healing agent that is encapsulated in the liquid core of the microcapsules. This determination should be done by performing other thermal analysis, such as MS-TGA and DSC experiments of the microcapsules to very low temperatures.

Given the initial poor quality of the coatings, a better coating formulation should be made while at the same time a better way to disperse the microcapsules should be found in order to get uniform and high quality coatings. These coatings need to give a better initial barrier protection. An improved way of applying the coating on the substrate could be by using an automatic wire wound applicator that gives a constant speed and pressure.

The reproducibility of the performed experiments should be tested, as it was not possible to get comparable results when doing the same experiment on different coatings. A major factor in the experiments is the application of the scratch. A method should be found to perform uniform (and thus comparable) micro and macro defects, which can be analysed whether they are able to heal.

When observing the applied scratch by means of AFM, it is of utmost importance that the exact same spot can be retrieved. A possibility is to use nano-indentation

to make small marks that can act as reference points in order to find back the same location and to be able to compare different AFM measurements of the same scratch. However, the risk exists that these indentations might disappear due to self-healing.

Bibliography

[1] R. Winston Revie, H. H. (2008). Corrosion and corrosion control: an introduction to corrosion science and Engineering. Hoboken, New Jersey: John Wiley and Sons.

[2] Gerhardus H.Koch, Michiel P.H. Brongers, Neil G. Thompson, Y. Paul Virmani, and J.H. Payer (2002). Corrosion costs and preventive strategies in the United States. Federal Highway Administration. Houston: McLean.

[3] S.J. Garcia, H. F. (2011). A critical appraisal of the potential of self healing polymers. Progress in Organic Coatings, p. 211-221.

[4] Iris De Graeve (2012). Brussels Retrofit XL - SHARC, Self-Healing Coatings in Architecture, Project Proposal.

[5] Y. Gonzalez-Garcia, J.M.C. Mol, T. Muselle, I. De Graeve, G. Van Assche, G. Scheltjens, B. Van Mele, H. Terryn (2011). A combined mechanical, microscopic and local electrochemical evaluation of self-healing properties of shape-memory polyurethane coatings. Electrochimica Acta, 56, p. 9619-9626.

[6] Y. Gonzalez-Garcia, J.M.C. Mol, T. Muselle, I. De Graeve, G. Van Assche, G. Scheltjens, B. Van Mele, H. Terryn (2011). SECM study of defect repair in self-healing polymer coatings on metals. Electrochemistry communications, 13, p. 169-173.

[7] J.B. Jorcin, G. Scheltjens, Y. Van Ingelgem, E. Tourwe, G. Van Assche, I. De Graeve, B. Van Mele, H. Terryn, A. Hubin (2011). Investigation of the self-healing properties of shape memory polyurethane coatings with the 'odd random phase multisine' electrochemical impedance spectroscopy. Electrochimica Acta, 55, p. 6195-6203.

[8] William D. Callister, David G. Rethwisch (2009). Materials Science and Engineering: An Introduction, 8th Edition. John Wiley and Sons.

[9] Robert G. Kelly, John R. Scully, David W. Shoesmith and Rudolph G. Buchheit (2003). Electrochemical techniques in corrosion science and engineering. New York: Marcel Dekker, Inc.

[10] Y. Van Ingelgem (2014). Course on corrosion and sustainability of materials.

[11] S. Van der Zwaag (2007). Self Healing Materials: An Alternative Approach to 20 Centuries of Materials Science. Springer.

[12] J. Boxall, J.A. von Fraunhofer (1980). Paint Formulation: Principles and Practice. George Godwin Limited, London, UK.

[13] Hill, Loren W. (1992). Structure/property relationships of thermoset coatings. Journal of coating technology, 64, nr. 808: p. 29-41.

[14] T. Vlček, H. Verbrugge, I. De Graeve, H. Pawlik (2013). Coatings with enhanced properties and prolonged lifetime. 4th Workshop on Green Chemistry and Nanotechnologies in Polymer Chemistry, Pisa.

[15] R. A. T. M. van Benthem, M. W. Ming, G. de With (2007). Self healing polymer coatings. Self-healing materials: an alternative approach to 20 centuries of materials science. Springer, Dordrecht, The Netherlands, p. 139-159.

[16] B.J. Blaiszik, S.L.B. Kramer, S.C. Olugebefola, J.S. Moore, N.R. Sottos and S.R. White (2010). Self-Healing Polymers and Composites. The Annual Review of Materials Research, 40, p. 179–211.

[17] T. Dikic (2006). Self-replenishing low-adherence polymer coatings. Ph.D. Thesis, University of Technology, Eindhoven.

[18] G. Scheltjens, J. Brancart, I. de Graeve, B. van Mele, H. Terryn, G. van Assche (2011). Self-healing property characterization of reversible thermoset coatings. Journal of Thermal Analysis and Calorimetry, 105, p. 805-809.

[19] S.D. Bergman, F. Wudl (2008). Mendable polymers. Journal of materials chemistry, 18, p. 41-62.

[20] D.Y. Wu, S. Meure, S. Solomon (2008). Self-healing property characterization of reversible thermoset coatings. Progress in polymer science, 33, p. 223-251.

[21] H. Otsuka, K. Aotani, Y. Amamoto, A. Takahara (2007). Thermal reorganization and molecular weight control of dynamic covalent polymers containing alkoxyamines in their main chains. Macromolecules, 40, p. 1429-1424.

[22] J. Canadell, H. Goossens, B. Klumperman (2011). Self-Healing Materials Based on Disulfide Links. Macromolecules, 44, p. 2536-2541.

[23] C. S. Coughlin, A. A. Martinelli, R. F. Boswell (2004). PMSE Preprints, 91, p. 472.

[24] S. J. Kalista, T. C. Ward, J. R. Soc. (2007). Interface, 4, p. 405.

[25] D. V. Andreeva, D. Fix, H. Mohwald, D. G. Shchukin (2008). Advanced Materials, 20, p. 1.

[26] L. Bouteiller (2007). Advanced Polymer Science, 207, p. 79-112.

[27] P. Cordier, F. Tournilhac, C. Soulie-Ziakovic, L. Leibler (2008). Nature, 451, p. 977-980.

[28] S. Burattini, H. M. Colquhoun, J. D. Fox, D. Friedmann, B. W. Greenland, P. J. F. Harris, W. Hayes, M. E. Mackay and S. J. Rowan (2009). Mutual binding of polymer end-groups by complementary π–π-stacking: a molecular "Roman Handshake". Chem. Commun, 44, p. 6717-6719.

[29] X. Luo, R. Ou, D.E. Eberly, A. Singhal, W. Viratyaporn, P.T. Mather (2009). Appl. Mater. Interfaces, 1, p. 612-620.

[30] S.A. Hayes, F.R. Jones, K. Marshiya, W. Zang (2007). Composites Part A, 38, p. 1116-1120.

[31] S.R. White, N.R. Sottos, P.H. Geubelle, J.S. Moore, M.R. Kessler, S.R. Sriram, E.N. Brown, S. Viswanathan (2001). Nature, 409, p. 794–797.

[32] S.D. Mookhoek, B.J. Blaiszik, H.R. Fischer, N.R. Sottos, S.R. White, S. van der Zwaag (2008). J. Mater. Chem., 18, p. 5390.

[33] S.H. Cho, H.M. Andersson, S.R. White, N.R. Sottos, P.V. Braun (2006). Adv. Mater., 18, p. 997.

[34] S.H. Cho, S.R. White, P.V. Braun (2009). Adv. Mater., 21, p. 645.

[35] A. Kumar, L.D. Stephenson, J.N. Murray (2006). Progress on Organic Coatings, 55, p. 244-253.

[36] M. Samadzadeh, S. Hatami Boura, M. Peikari, A. Ashrafi, S.M. Kasiriha (2011). Progress on Organic Coatings, 70, p. 142-149.

[37] Isophorone Diisocyanate. Wikipedia, the free encyclopedia. [Online] http:// http://upload.wikimedia.org/wikipedia/commons/e/e2/Isophorone-diisocyanate-2D-skeletal.png.

[38] E. Quérat, L. Tighzert, J.P. Pascault (1996). Microencapsulation of isocyanates. Characterization and storage stability of microcapsules in a polyster. Journal of Coating Technology, 68, p. 83-90.

[39] I.W. Cheong, JK. Kim (2004). Synthesis of core-shell polyurethane-urea nanoparticles containing 4,4'-methylenedi-p-phenyl diisocyanate and isophorone diisocyanate by self-assembled neutralization emulsification. Chem. Commun, p. 2484-2485.

[40] D. Sondari, A.A. Septevani, A. Randy, E. Triwulandari (2010). Polyurethane microcapsule with glycerol as polyol component for encapsulated self healing agent. International Journal of Engineering and Technology, 2, p. 466-471.

[41] J. Yang, M.W. Keller, J.S. Moore, S.R. White, N.R. Sottos (2008). Microencapsulation of isocyanates for self-healing polymers. Macromolecules, 41, p. 9650-9655.

[42] M. Huang, J. Yang (2011). Facile microencapsulation of HDI for self-healing polymers. Journal of Material Science, 21, p. 11123-30.

[43] B. Di Credico, M. Levi, S. Turri (2013). An efficient method for the output of new self-repairing materials through a reactive isocyanate encapsulation. European Polymer Journal, 49, p. 2467-2476.

[44] W. Wang, L. Xu, X. Li, Y. Yang, E. An (2014). Self-healing properties of protective coatings containing isophorone diisocyanate microcapsules on carbon steel surfaces. Corrosion Science, 80, p. 528-535.

[45] N. Birkner and Q. Wang (2013). [Online] How an FTIR spectrometer operates.
http://chemwiki.ucdavis.edu/Physical_Chemistry/Spectroscopy/Vibrational_Spectroscopy/Infrared_Spectroscopy/How_an_FTIR_Spectrometer_Operates

[46] K. Bartik (2012). Course on Molecular Structure and Material Characterization.

[47] A. W. Coats, J.P. Redfern (1963). Thermogravimetric Analysis: A Review. Analyst, 88, p. 906–924.

[48] Types of Differential Scanning Calorimetry (2004). [Online]
http://www.materialssolutions.info/thermal.html#

[49] TAM III (2014). [Online]
http://www.tainstruments.com/main.aspx?siteid=11&id=215&n=1

[50] N. Murasawa, H. Koseki, X. Li, Y. Iwata, T Sakamoto (2012). Study on Thermal Behaviour and Risk Assessment of Biomass Fuels. International Journal of Energy Engineering, 2, p. 242-252.

[51] B. Van Mele (2013). Course on Polymer Processing.

[52] E. McCafferty (2010). Introduction to Corrosion Science. Alexandria, USA, Springer.

[53] T. Burakowski, T. Wiezchon (1999). Surface Engineering of Metals: Principles, Equipment, Technologies. CRC Press.

[54] Interaction volume of an electron beam (2013). [Online]
http://www.ammrf.org.au/myscope/sem/background/concepts/interactions.php

[55] Atomic Force Microscopy. Wikipedia, the free encyclopedia. [Online]
http://en.wikipedia.org/wiki/Atomic_force_microscopy

[56] Diagram of an AFM. Wikipedia, the free encyclopedia. [Online]
http://upload.wikimedia.org/wikipedia/commons/5/5e/AFMsetup.jpg

[57] Wet Film Applicators. Gardco [Online]
http://www.gardco.com/pages/application/ap/wirewound_rods.cfm

[58] Principle of a wire-wound rod. Holoeast [Online]
http://www.holoeast.com/machines/coating/WIRE-WOUND-ROD.png

[59] The Fundamentals of Coating Thickness measurement. Paintgages [Online]
http://www.paintgages.com/The-Fundamentals-of-Coating-Thickness-Measurement-s/64.htm

[60] Klimatologisch overzicht van 2013. [Online]
http://www.meteo.be/meteo/view/nl/13812254-2013.html

[61] Equilibrium relative humidity of saturated salt solutions. Omega [Online]
http://www.omega.com/temperature/z/pdf/z103.pdf

[62] B. J. Blaiszik, N.R. Sottos, S.R. White (2008). Nanocapsules for self-healing materials. Composites Science and Technology, 68, p. 978-986.

Appendix

Synthesized prepolymers

Table 3: Synthesized prepolymers

Number	Date	Type	Solid content
1	7-10	GT	30 wt%
4	28-11	GT	30 wt%
6	10-12	COT	61 wt%
8	15-1	GT	27 wt%
9	10-2	GT	70 wt% -> 30 wt%
14	26-2	BT	44 wt%
18	12-3	GT	48 wt%
19	18-3	GT	69 wt% -> 30 wt%
20	7-4	GT	25 wt%

Synthesized microcapsules

Table 4: Synthesized microcapsules

Number	Capsules	Prepolymer	Date	Mixing	FTIR	SEM
1	GT-IPDI	7-10 (30 wt%)	8-10	Magnetic "Strong agitation"	YES	YES
2	GT-IPDI	7-10 (30wt%)	9-10	SON	YES	YES
3	GT-EMPTY	7-10 (30wt%)	12-11	SON	YES	YES
4	GT-IPDI	28-11 (30wt%)	10-12	Dispersion mixing head	YES	YES
5	GT-FD2	28-11 (30wt%)	11-12	Dispersion mixing head	YES	YES
6	COT-IPDI	10-12 (61 wt%)	11-12	Dispersion mixing head	YES	YES
7	COT-EMPTY	10-12 (61 wt%)	11-12	Dispersion mixing head	YES	YES
8	GT-FD2	15-1 (27 wt%)	3-2	SON	YES	YES
9	GT-IPDI	10-2 (70 wt%)	10-2	SON	YES	YES
10	GT-IPDI	10-2 (70 wt%)	13-2	SON	YES	NO
11	GT-IPDI	10-2 (70wt%)	17-2	SON	YES	YES
12	GT-HDI	10-2 (70 wt%)	26-2	SON	YES	YES
13	GT-HDI	10-2 (70 wt%)	26-2	Dispersion mixing	YES	YES

				head		
14	BT-IPDI	26-2 (44,4 wt%)	10-3	SON	YES	YES
15	BT-IPDI	26-2 (44,4 wt%)	12-3	SON	YES	YES
16	GT-IPDI	12-3 (48wt%)	18-3	Magnetic stirrer (500 RPM)	NO	NO
17	GT-IPDI	12-3 (48wt%)	19-3	Magnetic stirrer (350 RPM)	NO	NO
18	GT-IPDI	12-3 (48wt%)	19-3	Magnetic stirrer (800RPM)	NO	NO
19	GT-IPDI	18-3 (69wt%)	24-3	Magnetic stirrer (1200 RPM max)	YES	NO
20	GT-IPDI	7-4 (25,4 wt%)	8-4	SON	YES	NO
21	GT-EMPTY	7-4 (25,4 wt%)	9-4	SON	YES	NO

Synthesized coatings

Table 5: Synthesized coatings

Number	Wet thickness	Capsules	Coating mix	Substrate
1	100 µm	5 wt% GT-IPDI (son) 9october	Prepolymer 15january + glycerol	Q steel substrate (rinced w acetone+ethanol)
2	100 µm	5 wt% GT-IPDI (son) 9october	Prepolymer 15january + glycerol	Q steel substrate (rinced w acetone+ethanol)
3	500 µm	5 wt% GT-IPDI (son) 9october	Prepolymer 15january + glycerol	Q steel substrate (rinced w acetone+ethanol)
4	500 µm	5 wt% GT-IPDI (son) 9october	Prepolymer 15january + glycerol	Q steel substrate (rinced w acetone+ethanol)
5	100 µm	10 wt% GT-IPDI (son) 9october	Prepolymer 15january + glycerol	Q steel substrate (rinced w acetone+ethanol)
6	100 µm	10 wt% GT-IPDI (son) 9october	Prepolymer 15january + glycerol	Q steel substrate (rinced w acetone+ethanol)
7	500 µm	10 wt% GT-IPDI (son) 9october	Prepolymer 15january + glycerol	Q steel substrate (rinced w acetone+ethanol)

8	500 µm	10 wt% GT-IPDI (son) 9october	Prepolymer 15january + glycerol	Q steel substrate (rinced w acetone+ethanol)
9	100 µm	/	Prepolymer 15january + glycerol	Q steel substrate (rinced w acetone+ethanol)
10	500 µm	/	Prepolymer 15january + glycerol	Q steel substrate (rinced w acetone+ethanol)
11	100 µm	/	Alkyd resin	Q steel substrate (rinced w acetone+ethanol)
12	100 µm	/	Alkyd resin	Q steel substrate with Ti-conv pretreatment
13	100 µm	/	Prepolymer 15january + glycerol	Q steel substrate with Ti-conv pretreatment
14	100 µm	5 wt% GT-IPDI (son) 9october	Prepolymer 15january + glycerol	Q steel substrate with Ti-conv pretreatment
15	500 µm	5 wt% GT-IPDI (son) 9october	Prepolymer 15january + glycerol	Q steel substrate with Ti-conv pretreatment
16	500 µm	20 wt% GT-IPDI (son) 17 february	Prepolymer 50/50 19 february + glycerol	Q steel substrate with Ti-conv pretreatment
17	500 µm	20 wt% GT-IPDI (son) 17 february	Prepolymer 50/50 19 february + glycerol	Q steel substrate with Ti-conv pretreatment
18	500 µm	0 wt% Reference	Prepolymer 50/50 19 february + glycerol	Q steel substrate with Ti-conv pretreatment
19	500 µm	20 wt% GT-IPDI (son) 17 february	Prepolymer 18/3 (with extra cyclohexanone added)	Q-steel substrate with Ti-conv pretreatment + cleaning with acetone and drying (x3)
20	500 µm	20 wt% GT-IPDI (son) 17 february	Idem 19	Idem 19
21	100 µm	15 wt% GT-IPDI (son) 8/4	Prepolymer (25 wt%) 7april	Idem 19
22	500 µm	15 wt% GT-IPDI (son) 8/4	Prepolymer (25 wt%) 7april	Idem 19

23	100 µm	20 wt% GT-IPDI (son) 8/4	Prepolymer (25 wt%) 7april	Idem 19
24	500 µm	20 wt% GT-IPDI (son) 8/4	Prepolymer (25 wt%) 7april	Idem 19
25	100 µm	15 or 20 wt% GT-IPDI (son) 8/4	Prepolymer (25 wt%) 7april	Idem 19